

**PHOTO-CATALYTIC DEGRADATION OF  
METHYLENE BLUE AND MICRO-PLASTIC USING  
Mn AND Cu COBALTITE NANO-CATALYSTS**

Course code and Course Title: DISSERTATION (CGO-500)

Credits: 8

Submitted in partial fulfilment of Master's Degree

M.Sc. in Physical Chemistry

By

**Ms. SHIVANI VALLABH SAMANT**

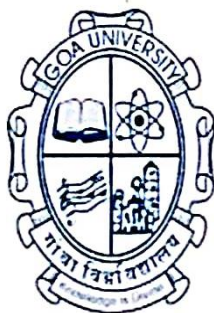
Roll Number: 21P049074

Under the Supervision of

**Dr. PRANAY P.MORAJKAR**

**School of chemical sciences**

**Physical chemistry**



Goa University

APRIL 2023



Seal of the School

Examined by:

*[Handwritten signatures]*  
Pranay P. Morajkar  
Shivani Vallabh Samant

## DECLARATION

I hereby declare that the data presented in this Dissertation report entitled, "Photo-catalytic Degradation of Methylene Blue and Micro-plastic Using Mn and Cu cobaltite nano-catalysts" is based on the results of investigations carried out by me in the Physical Chemistry at the School Of Chemical Sciences, Goa University under the Supervision/Mentorship of Dr. Pranay P. Morajkar and the same has not been submitted elsewhere for the award of a degree or diploma by me. Further, I understand that Goa University or its authorities will be not be responsible for the correctness of observations / experimental or other findings given the dissertation.

I hereby authorize the University authorities to upload this dissertation on the dissertation repository or anywhere else as the UGC regulations demand and make it available to any one as needed.

Signature and Name of Student: <sup>Shivani</sup> Shivani Vallabh Samant

Roll Number/Seat no: 21P0490714  
Name of Discipline: Physical chemistry  
Name of School: School of Chemical Sciences

Date: 29/4/2023

Place: Goa University

## CERTIFICATE

This is to certify that the dissertation / internship report "Photo-catalytic Degradation of Methylene Blue and Micro-plastic Using Mn and Cu cobaltite nano-catalysts" is a bonafide work carried out by Ms. Shivani Vallabh Samant under my supervision/mentorship in partial fulfilment of the requirements for the award of the degree of Master Of Science in the Discipline Physical Chemistry at the School Of Chemical Sciences, Goa University.

  
Dr. Pranay P. Morojkar

Signature and Name of Supervising Teacher/ Mentor for internship  
Name of Discipline

Date: 24/4/2023



School Stamp

  
29/4/2023  
Prof. V. M. S. Verenkar

Signature and Name of Dean of the School

Name of Discipline : physical chemistry

Name of School : School of Chemical Sciences

Date: 24/4/2023

Place: Goa University

## **ACKNOWLEDGEMENT**

I take this opportunity to express my profound gratitude and sincere thanks to my guide, Dr. Pranay P.Morajkar, for his constant help and guidance throughout my dissertation work. I would also like to extend my sincere gratitude to Ms.Sarvesha Shetgaonkar for her constant support and guidance.

I am grateful to Ms. Samantha Da Costa, Ms. Bernice Viegas, Mr. Mohit Mainikar and Ms. Dwana Martins for helping me out during my dissertation work .I also thank all the teaching and non-teaching staff of School of Chemical Sciences, Goa University for their valuable help during the course of the work. Lastly I would like to thank my parents for their constant support.

## TABLE OF CONTENTS

|                                                                                                      |          |
|------------------------------------------------------------------------------------------------------|----------|
| <b>ABSTRACT.....</b>                                                                                 | <b>7</b> |
| <b>KEYWORDS.....</b>                                                                                 | <b>7</b> |
| <b>HIGHLIGHTS.....</b>                                                                               | <b>8</b> |
| <b>CHAPTER I</b>                                                                                     |          |
| 1.0 Introduction.....                                                                                | 10       |
| 1.1 Photo-catalysis by metal oxides.....                                                             | 14       |
| 1.1.1 Photo-catalysts used for degradation of methylene blue and micro-plastics degradation<br>..... | 16       |
| 1.1.2 Cobaltites as photo-catalyst.....                                                              | 18       |
| 1.1.3 Methods of synthesis.....                                                                      | 19       |
| 1.2.0 Literature survey on photo-catalytic degradation of common micro-plastics &<br>dyes.....       | 19-43    |
| 1.2.1 Low-density polyethylene.....                                                                  | 20       |
| 1.2.2 Polystyrene .....                                                                              | 24       |
| 1.2.3 Polyethylene terephthalate (PET) .....                                                         | 28       |
| 1.2.4 Polypropylene.....                                                                             | 30       |
| 1.2.5 High Density Polyethylene (HDPE).....                                                          | 33       |
| 1.2.6 Polyethylene.....                                                                              | 34       |
| 1.2.7 Methylene blue as water pollutant.....                                                         | 40       |
| 1.3 Thesis objectives.....                                                                           | 42       |

## **CHAPTER II**

|                                                                             |           |
|-----------------------------------------------------------------------------|-----------|
| <b>2.0 Prologue.....</b>                                                    | <b>44</b> |
| 2.1 Materials used .....                                                    | 44        |
| 2.2 Protocols for co-precipitation synthesis of $Mco_2O_4$ (M= Mn, Cu)..... | 44-47     |
| 2.3 Pristine condition.....                                                 | 44        |
| 2.4 Using structure directing agents(SDA).....                              | 45        |

## **CHAPTER III**

|                                                    |           |
|----------------------------------------------------|-----------|
| <b>3.0 Prologue.....</b>                           | <b>49</b> |
| 3.1 Instrumentation.....                           | 49        |
| 3.2 Characterization of $MnCo_2O_4$ Catalyst ..... | 52-58     |
| 3.3 Characterization of $CuCo_2O_4$ Catalyst.....  | 58-62     |

## **CHAPTER IV**

|                                                            |              |
|------------------------------------------------------------|--------------|
| <b>4.0 Photo-catalytic activity test.....</b>              | <b>64-67</b> |
| 4.1 Photocatalytic degradation of Methylene Blue.....      | 64           |
| 4.2 Photocatalytic degradation of LDPE micro-plastics..... | 65           |
| <b>CONCLUSION.....</b>                                     | <b>68</b>    |
| <b>BIBLIOGRAPHY.....</b>                                   | <b>69</b>    |

## **ABSTRACT**

In this study of Metal Cobaltites,  $\text{MnCo}_2\text{O}_4$  and  $\text{CuCo}_2\text{O}_4$  were synthesized by Co-precipitation method using urea and semicarbazide as structure directing agents (SDA). Photo-catalytic activity of the synthesized catalysts was analyzed using 250 Watts UV source. The catalysts were characterized using FTIR, XRD, UV-DRS, SEM and C,H,N S Elemental analysis. Their photo-catalytic ability was determined by degrading dye such as methylene blue (MB) and micro-plastic (LDPE). Findings indicate that manganese and copper cobaltites synthesized using semicarbazide SDA showed highest degradation of 18.43%, for MB dye and micro-plastic respectively. This can be due to its small crystallite size, better morphology (microspheres) and band gap of 2.1eV. In case of micro-plastic degradation, the degradation may be facilitated due its band gap of 1.5 eV, The degradation was confirmed using SEM and it showed cleavage formation on the surface of the micro-plastic (LDPE).

## **KEYWORDS:**

Photo-catalysis, Micro-plastic, Methylene Blue,  $\text{MnCo}_2\text{O}_4$ ,  $\text{CuCo}_2\text{O}_4$

## **HIGHLIGHTS:**

1) Dyes are prominently used in textile industries. methylene blue is a cationic dye which when left in water bodies untreated is a threat to humans and aquatic flora and fauna. Micro-plastics being difficult to detect due to their small dimensions between 0.1  $\mu\text{m}$  and 5 mm can easily enter the food chain and threatening the life of living organisms.

2) Mixed metal cobaltites due to their easier availability, ability to successfully degrade pollutants photo-catalically, and since their band gap is in visible region (1.5 eV to 2.1eV) were used to degrade dye (MB) and micro-Plastic (LDPE).

3) Metal cobaltites synthesized using Co-precipitation method gives high yield. Microspheres morphology was seen for  $\text{MnCo}_2\text{O}_4$  synthesized using semicarbazide SDA.

4) It is observed that  $\text{MnCo}_2\text{O}_4$  and  $\text{CuCo}_2\text{O}_4$  synthesized using semicarbazide show better photo-catalytic activity in degradation of methylene blue dye and micro-plastic respectively using a 250 watts UV source in a photo reactor.

# CHAPTER I

## **1.0 Introduction**

Water pollution has been a major concern for 21<sup>st</sup> century. From the relentless cutting of trees, smoke released from automobiles to release of harmful chemicals in the water, getting pollution under control has been a nearly impossible task. Methods such as limited use or banning of harmful products only succeed partially, since most of these items have high demand and are necessary for daily life. The disposing of raw materials used in the synthesis of such products is a major issue. Dyes and plastic are prominent examples.

Dye contaminants are prominently disposed from various textile, food and leather industries into the natural water systems leading to contamination. Amaranth, Methylene blue, Rhodamine B, Methyl orange etc. are some major dyes. Methylene Blue (MB) is an intensely coloured compound which is used in dyeing and printing textiles and is a common water pollutant. In most cases the MB infected waste water left in the nearby water bodies may result in eutrophication and perturbations in the aquatic life. It is carcinogenic to humans as well.

Plastic, a long-chained polymer was invented for the convenience of mankind. Its valuable characteristics such as lightweight, excellent chemical stability, high durability, and low cost made it an excellent alternative for industries to produce toys, bags, etc<sup>1</sup>. Over the past 60 years, plastic production has multiplied 560 times<sup>2</sup>. Due to its high resistance to biodegradation, plastic accumulation has become one of the biggest threats to the environment. This stability of plastics, can be explained in terms of its high molecular weight and hydro-phobicity<sup>3</sup>. The increasing production of single use plastics for packaging of various consumer goods, is mainly responsible for its accumulation in the environment<sup>2</sup>. The Global production of plastic (excluding fibres) increased from 1.3 million tons in 1950 to 359 million tons (including Polypropylene (PP) fibres) in 2018<sup>4</sup>. About 58% of the plastics produced are being disposed into the natural ecosystem; leading to ecological imbalance. It is

further preserved in a solid form for long term. It's observed that only about 18% of the plastic is recycled and 24% is burnt<sup>2</sup>. Under the influence of biological, chemical, and physical processes macro-plastic gets broken down in a slow process to form micro-plastics<sup>4</sup>.

Plastic particles with a size between 0.1  $\mu\text{m}$  and 5 mm are generally known as micro-plastics<sup>5</sup>. They are found in various shapes such as spheres, fragments, and fibres. They are segregated as primary and secondary micro-plastics. The primary micro-plastics include industrial products such as cosmetics as well as different kinds of textiles, while secondary plastics is a result of fragmentation of larger plastics<sup>6</sup>. These micro-plastic particles can further break down over a period of time to give nano-plastics. Besseling et al.<sup>7</sup>(2018) estimated that a spherical micro-plastic can generate more than  $10^{14}$  nano-particles. In the future, these micro-plastics will be humanity's one of the biggest concerns. The threat posed by them far exceeds that posed by macro-plastics, few of the reasons are the ease with which they can spread in the environment given the size and can enter the food chains of living organisms leading to severe health problems, the high surface area for adsorption of contaminants<sup>8</sup> make micro-plastics a potential carrier of toxins causing environmental destruction. The stability of micro-plastics can be understood from the fact that Cauwenberghe et al.<sup>9</sup> found, for the first time, the presence of micro-plastics at the bottom of the oceans.

Humans have devised various ways to curb this ongoing plastic pollution such as reducing, recycling, and reusing, but the greed of humans has engrained plastic in our environment at a microscopic level rendering these simple plastic prevention techniques useless. A way has to be devised to degrade plastic not only at a macro stage but also micro stage. Micro-plastics are stable hence degrading them is difficult. The natural decomposition of micro-plastic can take decades and in the process will release a diversity of hazardous organic substances from polymers and other additives such as plasticizer and anti-oxidizer in manufacturing.

Transport of micro-plastics can occur through various methods including wastewater inputs, runoff from roads and sealed surfaces, or inappropriate waste management<sup>3</sup>. Since most of the earth is covered in water bodies it becomes one of the major transport systems for micro-plastics. A recent study has revealed that more than 100 billion micro-plastics can be released by a single wastewater treatment plant yearly<sup>6</sup>. It has been observed that even after treatment of wastewater before release, it cannot completely remove the plastic in it. This problem worsens as residuals of this treatment process can be used in agriculture, providing a passage for micro-plastics to end up in the soil and potentially the groundwater resources via other pathways which we have limited understanding of<sup>3</sup>.

Many techniques have been used to degrade micro-plastics, which can be segregated into abiotic and biotic degradation techniques. Biotic methods include the fragmentation of micro-plastics into small sizes with the help of microbes. The biodegradation process is categorized into conditional film formation, colonization, bio-fragmentation, assimilation, and mineralization. These processes rely on plastic's molecular weight, crystal structure, functional groups, and additives. It can occur aerobically producing CO<sub>2</sub> and H<sub>2</sub>O as well as anaerobically where CH<sub>4</sub> is produced additionally. Abiotic degradation can be further subdivided into mechanical, thermal, and chemical methods. The mechanical method is a result of the abrasion of micro-plastics caused by interaction with debris. When this was tested through experimentation PE and PP showed a lower likelihood of undergoing mechanical stress, while expanded polystyrene was more prone to it. Thermal degradation gained popularity due to its ability to provide an alternative source of fuel<sup>10</sup>. It has also been observed that this method is useful in the case of mixed or contaminated plastic waste<sup>9</sup>. The disadvantages include minimal heat transfer and low diffusion capacity. Recent attempts have been made to use supercritical water to increase thermal degradation efficiency. Chemical techniques are dependent on additives, polymers, medium, and depositional settings. The

range of absorbance of micro-plastics changes depending on the environment. Presence of oxygen and UV radiation results in photo-degradation. From the data observed it can be said that PP(Polypropylene),PS (Polystyrene),PE(Polyethylene), and PVC (Polyvinyl chloride) degradation rate is slower compared to PET. The reason stated is the resistance to photo-oxidation shown by C-C bonds. In PE and PP, the C-H bond is broken due to either UV radiation or thermal degradation giving free radicals to react with oxygen.This process forms inert products and reduces the molecular weight of the polymers,which can further undergo mechanical or biological degradation. Hydrolysis is another method occurring when the above-mentioned processes cannot occur, like in landfills or ocean floors.The aromatic polyesters hydrolyze forming shorter chains leading to the formation of terephthalic acid and ethylene glycerol<sup>10</sup>. Among these various degradation techniques photo-catalysis is gaining popularity due to its innovative and environment-friendly approach.

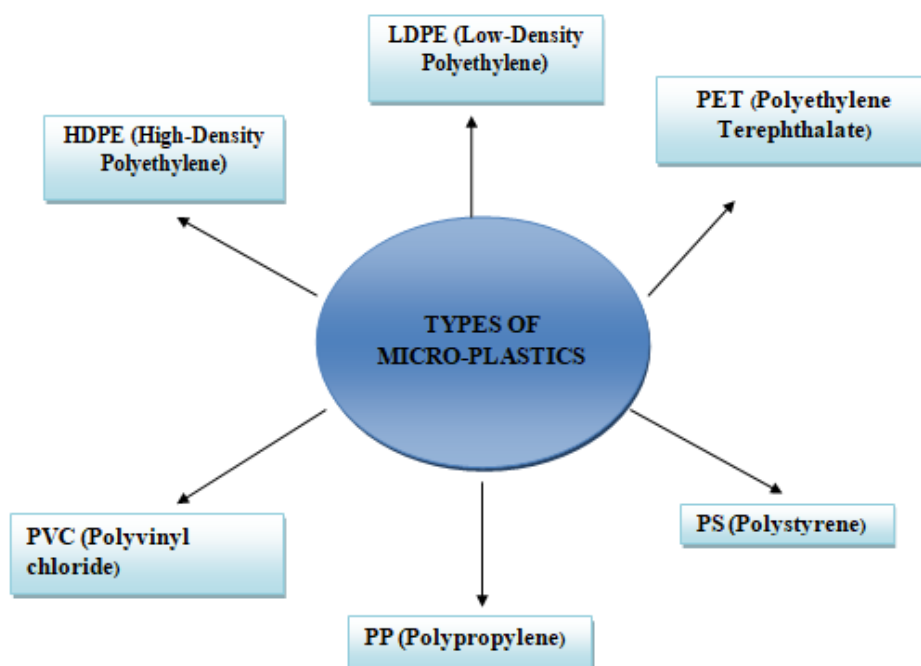


Figure 1: Schematic depicting the types of micro-plastics

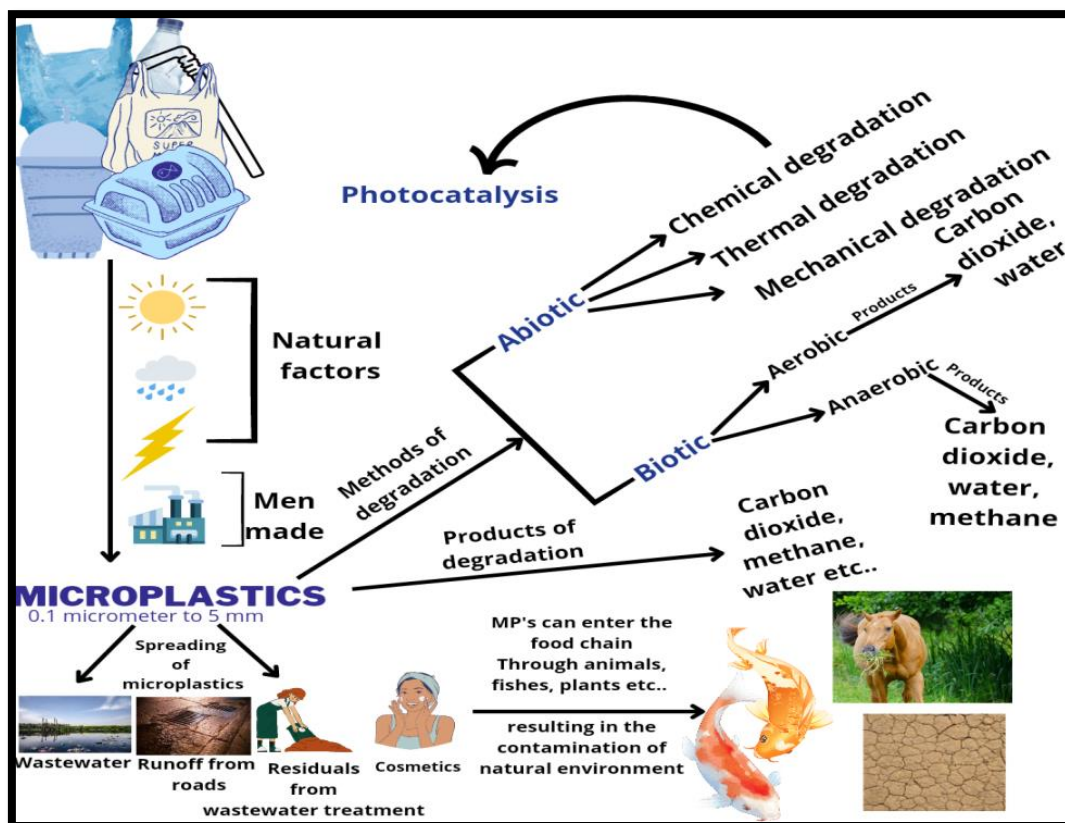


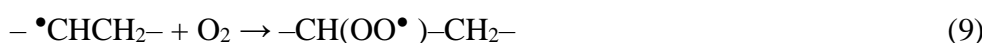
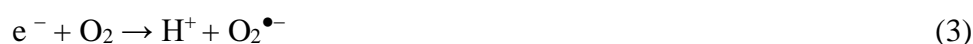
Figure 1.1: Schematic illustration of degradation of plastic

### 1.1 Photo-catalysis by metal oxides

In 1972, the discovery of photo-catalytic splitting of water on  $\text{TiO}_2$  electrode, opened the world to an economical and environment friendly technique, photo-catalysis. Photo-catalysis uses the naturally available solar energy to catalytically degrade plastics into simpler products, thus simultaneously addressing the problems of environmental pollution and world energy crisis. This technique has already been used for  $\text{H}_2$  production via photo-catalytic water splitting, dye-sensitized and organic solar cells, and photo-sensitizers in photovoltaic devices<sup>9</sup>. As mentioned earlier using photo-catalysis for micro-plastic degradation would be a major win for the environment.

Photo-catalysis includes three main steps: (1) Absorption of light (2) Separation and migration of photo-induced electrons and holes (3) Redox reaction on the surface of the

photo-catalyst<sup>9</sup>. The degradation can be achieved by direct or indirect mechanism. The indirect mechanism initiates with the excitation of electrons from the valence band to the conduction band, after irradiation of light containing photons that possess energy greater than or equal to the band gap. This leaves holes behind in the valence bands as shown in equation 1<sup>8</sup>. Recently, Llorente-García et al. and Zhao et al<sup>9</sup>. have proposed the general mechanism of photo-degradation of MPs, such as PE as follows:



The electron-hole pairs formed, migrate to the interface yielding active radicals such as hydroxyl ( $\bullet\text{OH}$ ), hydroperoxy ( $\text{HO}_2^\bullet$ ), superoxide ( $\text{O}_2^{\bullet-}$ ) radicals. The hydroxyl radical breaks the C-H bonds giving polyethylene alkyl radicals ( $-\bullet\text{CHCH}_2-$ ). During propagation alkyl radical formed reacts with oxygen to create peroxy radicals ( $-\text{CH}(\text{OO}^\bullet)-\text{CH}_2-$ ) which removes hydrogen from another alkyl group forming hydroperoxide species. Then, the

hydroperoxide is further cleaved into two new free oxy radicals ( $-\text{CHO}^\bullet-\text{CH}_2-$ ) and hydroxyl radicals ( $\text{OH}^\bullet$ ) by the scission of the weak O–O bond. The propagation step ultimately leads to chain scission, resulting in a lower molecular weight. The radicals formed could react further to give low-molecular-weight fragments such as carboxylic acids, alcohols, aldehydes, ketones, and carboxylates. Zhao et al. demonstrated that photo-degradation of PE is an environment-friendly process in which  $\text{CO}_2$  was the primary product<sup>9</sup>. A study of the direct mechanism can be done by taking  $\text{TiO}_2$  as a photo catalyst, since the band gap between valence band and conduction band is small, between 3.0 to 3.2 eV<sup>8</sup>.



Direct degradation of plastic occurs under visible light in the presence of  $\text{TiO}_2$ . The excited state of plastics forms semi-oxidized cation radicals through  $e^-$  injection in the Conduction Band of the catalyst. The trapped electrons react with dissolved oxygen leading to the formation of  $\text{O}_2^{\bullet-}$  which subsequently forms  $^\bullet\text{OH}$  that is responsible for the target pollutant's decomposition. This mechanism is slower as compared to the UV light-based reactions<sup>8</sup>.

### **1.1.1 Photo-catalysts used for degradation of methylene blue and micro-plastics degradation**

Research on micro-plastic degradation using photo-catalysis has started recently; hence the work done on it is limited. Where dyes have been widely used for photo-catalytic degradation. The important characteristics of a photo catalyst are desired band gap, suitable morphology, high surface area, stability, and reusability. Oxides of vanadium, titanium, zinc,

tin, cerium, and chromium are well known photo-catalyst, among which ZnO and TiO<sub>2</sub> are most common. The favourable combination of electronic structure, light absorption properties, charge transport characteristics, and excited lifetimes of metal oxides have made it possible for their application as photo-catalysts<sup>11</sup>. This is explained by their excellent stability under a wide range of circumstances, biocompatibility, and capacity to produce charge carriers when stimulated with the necessary quantity of light energy. Metal sulphides are another well known class of photo-catalysts, having a lesser band gap as compared to metal oxides but also having lower stability as compared to oxides under photo-catalytic conditions. The morphology and synthesis method of the catalysts used also influences their photo-catalytic capabilities. ZnO, TiO<sub>2</sub>, ZnS, CdS, SrO<sub>2</sub>, WO<sub>3</sub> etc are a few of the photo-catalysts. Among these ZnO and TiO<sub>2</sub> are widely used for micro-plastic and dye degradation in various forms such as ZnO in the form of nanorods and nano-particles, ZnO nanorods immobilized onto glass fibers or supported on platinum nano-particles to enhance the activity. TiO<sub>2</sub> nano-particles as well as nanotubes are very popular, C-TiO<sub>2</sub> nano-particles, N-TiO<sub>2</sub> nano-particles, etc are prepared by doping. Hybrids such as Bi<sub>2</sub>O<sub>3</sub>@N-TiO<sub>2</sub> are popular photo-catalysts. Heterojunction photo-catalysts are also widely used. They are basically defined as the interface between two types are semiconductors which differ in band structure causing alignment of the bands<sup>12</sup>. Mixed metal oxides have been under study for their wide applications as photo-catalysts as a result of their high surface area and reactive sites. Thin films were developed by doctor blade deposition of Cu<sub>x</sub>S and Cu<sub>x</sub>S/TiO<sub>2</sub> composites having photo-catalytic properties. It was observed that the semiconductors association and the films homogeneity limit the electron-hole recombination, resulting in their good efficiency in dyes photo degradation even under visible light irradiation<sup>13</sup>.

### **1.1.2 Cobaltites as photo-catalysts**

As mentioned in the previous section mixed metal oxides possess wide applications owing to their high surface area and reactive sites<sup>13</sup>. Among them transition metal oxides exhibit unique physical and chemical properties. These nano-composites have unique attractive properties, which might be due to their small size. The various magnetic properties make them an interesting choice in fields ranging from medicine to photo-catalysis. When transition metal oxides were experimented with for the activation of PMS they showed promising results. CuO, Fe<sub>3</sub>O<sub>4</sub>, MnO<sub>2</sub>, Mn<sub>3</sub>O<sub>4</sub> and Co<sub>3</sub>O<sub>4</sub> produced many active radicals for degrading refractory organic pollutants<sup>14</sup>. Cobalt oxide (Co<sub>3</sub>O<sub>4</sub>) is an important magnetic and P-type semiconductor<sup>15</sup> and according to Kim et al. Cobalt oxides have been widely used to solve environmental problems and photo-reduction of CO<sub>2</sub><sup>16</sup>. Yong sheng Yan and et al. prepared carbon modified Co<sub>3</sub>O<sub>4</sub> /BiVO<sub>4</sub> p-n heterojunction photo-catalyst (Co<sub>3</sub>O<sub>4</sub> /BiVO<sub>4</sub>/C) in order to enhance light absorption. It was seen that this modified product showed higher degradation efficiency of tetracycline in visible light than that of pure Co<sub>3</sub>O<sub>4</sub> and BiVO<sub>4</sub><sup>15</sup>. The combination of two semiconductor nano-materials displayed properties of both nano-materials such as the increase in charge carrier's photo-generation process<sup>17</sup>. Manganese is an abundant material with low cost and range of chemical valence states making itself an obvious choice to create mixed metal oxides. Cobalt oxide combined with Manganese has a variety of valence states, which is conducive to redox reaction<sup>14</sup>. Along with Manganese, Copper is also an abundant, low cost metal has attracted considerable attention. P-type semiconductor CuCo<sub>2</sub>O<sub>4</sub> electrode along with the above mentioned benefits also showed high conductivity, resistance to corrosion and non-toxicity. When compared with copper's single metal oxides CuO or Co<sub>3</sub>O<sub>4</sub> form, its ternary compound CuCo<sub>2</sub>O<sub>4</sub> showed higher electrochemical activity and conductivity which can be attributed to the lower activation energy of charge transfer in multivalent transition metal cations. Recently CuCo<sub>2</sub>O<sub>4</sub> is

gaining attention of researchers for photo-catalysis. It has been used in degradation of methyl orange, reduction of hexavalent chromium and CO<sub>2</sub> etc<sup>18</sup>. With the problems due to micro-plastics rising, these MnCo<sub>2</sub>O<sub>4</sub> and CuCo<sub>2</sub>O<sub>4</sub> can be useful photo-catalysts for degradation of micro-plastics since they have shown good results in degradation of other pollutants. Sadly this research is fairly new and is yet to see proper progress. Using these low cost, abundant metals interinary form such as MnCo<sub>2</sub>O<sub>4</sub> and CuCo<sub>2</sub>O<sub>4</sub> might help solving this MB and micro-plastic crisis, but more research on their ability to degrade MB and micro-plastic is needed.

### **1.1.3 Methods of synthesis**

As mentioned in the previous section methods of synthesis greatly affects the photo-catalytic ability of the catalyst. Methods for synthesis predominantly include hydrothermal method, solvothermal method, sol gel synthesis, and co-precipitation among others. The popularity of hydrothermal method stems from its ability to produce a controlled design of multi-dimensional photo-catalysts. It also provides other advantages such as high crystallinity and morphology control. It is low cost as compared to sol-gel method, which requires expensive precursors and solvents. When compared to hydrothermal method, solvothermal method uses non-aqueous solvents which expands the range of solvent-based raw materials<sup>19</sup>. But the yield in case of hydrothermal synthesis is less since limited amount of precursor weights can be used. Whereas in co-precipitation is an efficient method giving higher yield in a lesser time with better quality.

### **1.2.0 Literature survey on photo-catalytic degradation of some commonly encountered micro-plastics:**

As seen in figure 1 there are various types of micro-plastics. Since the degradation of micro-plastic by photo-catalysis is a recently researched topic, few catalysts have been tried for the

aforementioned application. In this article, we have tried to shed a light on the different types of micro-plastics and the photo-catalysts used for their degradation as seen in table 1.1.

### **1.2.1 Low-density polyethylene**

Low-density Polyethylene (LDPE) was originally synthesized by high-pressure polymerization of ethylene. The global usage of LDPE has resulted in its accumulation in the environment. In an experiment, it was observed that a polyethylene sheet, kept in moist soil for 12 years showed no confirmed weight loss<sup>20</sup>. Photocatalytic degradation has been attempted on this category of micro-plastics. The various photo-catalysts used include ZnO nanorods, ZnO nanorods-supported platinum nano-particles, Polyacrylamide-grafted ZnO nano-particles, N-TiO<sub>2</sub>, TiO<sub>2</sub> nano-tubes and nano-particles, Carbon and Nitrogen doped TiO<sub>2</sub> nano-particles, spinel NiAl<sub>2</sub>O<sub>4</sub>.

As can be seen, zinc and titanium oxides are predominantly used as photo-catalysts, this can be attributed to their band gaps which are approximately 3.37 eV and 3.1 eV respectively, and the ease of synthesizing their oxides in a desired shape<sup>21</sup>. Ali et al. observed that the TiO<sub>2</sub> nano-particles possess 81 m<sup>2</sup>/g surface area as compared to TiO<sub>2</sub> nanotubes possessing 161 m<sup>2</sup>/g, showing efficiency of 67% for photo-catalytic degradation under UV radiation. TiO<sub>2</sub> nanotubes with an average size of 40 nm showed degradation efficiency of 78% when irradiated with UV radiation from 18W ultraviolet lamps for 15 days. Since TiO<sub>2</sub> is active only in UV wavelength (below 385 nm), to utilize the visible part of solar energy it was sensitized with a brilliant green dye. 10% Dye-sensitized TiO<sub>2</sub> nanotubes showed 48 % degradation efficiency and dye-sensitized nano-particles showed an efficiency of 41% in visible light over a period of 45 days. The advantage of dye sensitized TNT is its ability to produce more  $\cdot\text{OH}$  to the photo-degrade polymer matrix. Due to the ability of dye sensitized TiO<sub>2</sub> to degrade in visible light; this LDPE-TNTs composite can be an environmentally

friendly alternative to other polymer materials. Even though the use of dye enhances the degradation efficiency of TiO<sub>2</sub> in visible light, it is still inferior to the degradation caused by TiO<sub>2</sub> nanotubes in UV light<sup>22</sup>. Mesoporous coating of N-TiO<sub>2</sub> was also used in an attempt to photo-catalytically degrade LDPE. The problem observed in the photo-catalysis of these Microparticles was dealing with limited or null adsorption shown by large particles of micro-plastic on the semiconductor. Collisions between the irradiated coating and the micro-plastics additionally cause the infiltration of •OH and O<sub>2</sub> radicals from the N-TiO<sub>2</sub> surface into the reaction medium enables their interaction with the scattered microplastics, ultimately causing deterioration of the plastic. (due to stirring) can lead to contact between surface-bound ROS and micro-plastic particles. According to Llorente-Garcia et al., N-TiO<sub>2</sub> coating was done by the evaporation-induced self-assembly method. The test was performed in an aqueous medium contaminated with micro-plastics, at pH 3, by exposing the system to visible light using a 50 W LED Lamp. Due to the inherent presence of chromophoric groups, photo-initiated degradation could occur to some extent but the mass losses observed weren't significant enough. A Mass loss of 4.65% was observed after 50 hrs of irradiation. It was seen that the interaction between the micro-plastics and the clean glass substrates added, did not promote mass loss of the plastics due to mechanical action, but stirring it induced the formation of buoyant LDPE micro-plastic films in the liquid–gas interface of the reaction system, resulting in a layer of micro-plastic. This micro-plastic layer could affect the photo-catalytic process negatively and hinder the absorption of light by the N–TiO<sub>2</sub> coating immersed in the buffer and it could also decrease the diffusion efficiency of oxygen into the liquid phase. The experiment also showed the high durability of LDPE in an acidic environment<sup>23</sup>.

Hydrothermally synthesized ZnO nanorods were used to degrade LDPE in visible light using a 50 W dichroic halogen lamp in ambient air. The initiation of degradation was again a result

of the Chromophoric groups, manufacturing defects, and weak links providing sites for the oxidation process, in turn leading to the degradation of the molecular bonds after photocatalytic exposure for a significant amount of time. The longer the rods higher will be the surface area, hence generating a higher number of radicals for better photo-degradation. The nanorods are 250 to 1750 nm long varying in width from 34 to 65 nm for the precursor concentrations of 3 mM, 5 mM, 10 mM, and 20 mM, leading to the total effective surface area of 6.5, 22, 49, and 55 cm<sup>2</sup> respectively. The alkoxy radicals generated in this degradation process successively produce carbon and vinyl groups giving a rough estimate of the extent of degradation. It is observed that for precursor concentration of 20 mM, the carbonyl index is 1.51 and the vinyl index is 1.3. These groups can further undergo oxidation to produce carbon dioxide and water<sup>21</sup>. ZnO nanorods-supported platinum nano-particles (ZnO-Pt) synthesized by the UV-C photo-reduction method give a carbonyl index value of 1.49 and vinyl index value of 1.35 as per Tofa et al. The deposition of platinum nano-particles on the zinc nanorods enables it to effectively degrade micro-plastic particles which are a result of the plasmonic effect leading to better interfacial exciton separation and improved hydroxyl radical activity along with a 78% increase in visible light absorption. The plasmonic metal deposition on ZnO reduced the recombinations of electron-hole pairs and enhanced the absorption of visible light. The synthesized ZnO nanorods and ZnO-pt were approximately of the size 55 μm and 960 μm. It was observed that ZnO nanorods show strong absorption in the UV region but after the platinum deposition there was about 78% increase in the visible light absorption which could be due to the surface plasmon resonance effect. A reduction in the ZnO band-to-band excitation at 362 nm was noted which might be the result of increased defect density in the ZnO nanorod, due to the exposure of ZnO to the UV-light before platinum deposition, and reduced light intensity incident on the surface of ZnO. These factors result in the improvement of the absorption in the visible region<sup>24</sup>. The ultrasonication

method was employed to synthesize Polyacrylamide-grafted ZnO nano-particles. The grafting of polyacrylamide on the surface of ZnO nano-particles enhances the dispersion and boosts photo-catalytic activity. It increases the hydrophilicity in the LDPE matrix in turn facilitating the degradation process. UV light Lamps with a power of 30 W (350–280 nm) were used as the light source for photo-catalytic degradation. The grafting process was done for 10% and 39% polyacrylamide. The absorption showed a decrease for 39% grafting because increasing the number of polymers on the surface of the nano-particles, decreases the UV absorption rate. One of the reasons might be the decrease in the density of the existing chains in the nano-particles, which might prevent the light from reaching the surface of the nano-particles decreasing the photo-catalytic activity. The Degradation efficiency varies with time, 50, 100, and 200 minutes and gives 7%, 14.6% and 25% respectively<sup>25</sup>.

There is a lack of abundant studies on the preparation of spinel compounds using hydrothermal and co-precipitation methods. Nickel provides an enhanced catalytic system with low costs; hence NiAl<sub>2</sub>O<sub>4</sub> was prepared and used for photo-catalysis under the metal halide lamp of 350 W as a source for the visible light. The average size of the compound formed using the hydrothermal method and co-precipitation was 31.7 nm and 42.6 nm respectively. They have band gaps of 2.57 eV and 2.757 eV respectively. It was observed that spinels formed from co-precipitation didn't show absorption in visible range whereas spinels formed from the hydrothermal method had maximum absorption in the visible range facilitating photo-degradation. The process of degradation of LDPE using NiAl<sub>2</sub>O<sub>4</sub> results in the formation of carbon dioxide and water<sup>26</sup>. Figure 1.2 showcases the morphology of few of the photo-catalysts mentioned above.

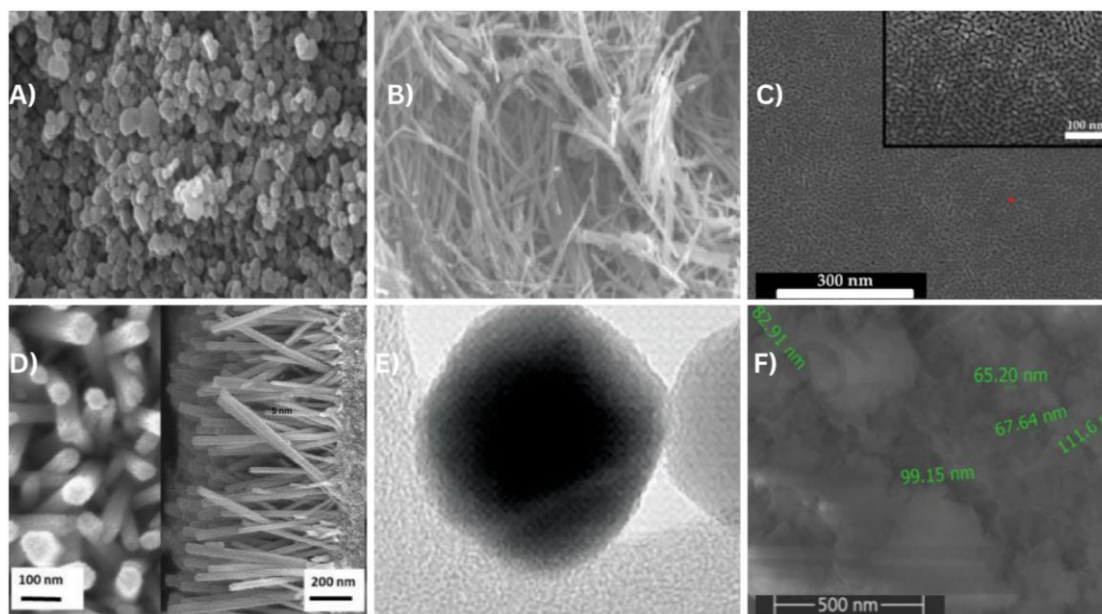


Figure 1.2: SEM image of TiO<sub>2</sub> nano-particles (A), SEM image of TiO<sub>2</sub> nanotubes (B), FEG-SEM micrographs of N-TiO<sub>2</sub> coating microstructure (C), SEM image of platinum nano-particles-deposited on ZnO nanorods (D), TEM micrographs polyacrylamide grafted ZnO nano-particles (E), SEM micrograph of hydrothermally prepared spinels NiAl<sub>2</sub>O<sub>4</sub> (F). (Reproduced from Elsevier, <sup>22</sup>, <sup>26</sup>, <sup>25</sup>)

### 1.2.1 Polystyrene

A form of plastic made from petroleum called polystyrene contains the deadly carcinogen benzene. Polystyrene is most commonly used in the production of insulators and packaging materials<sup>27</sup>. The photo-catalysts used in the degradation of polystyrene microspheres include TiO<sub>2</sub> nano-particles under the irradiation of UV light to produce carbon dioxide, water and carbon monoxide. Nabi et al. observed that TiO<sub>2</sub> nano-particles film made with Triton X-100, when placed under the UV light for 12 hours gave mineralization of 98% of the polystyrene (400 nm). TXT proved to be the better option in terms of generation, separation, and transport of electron-hole pairs as can be seen in figure 1.3<sup>28</sup>.

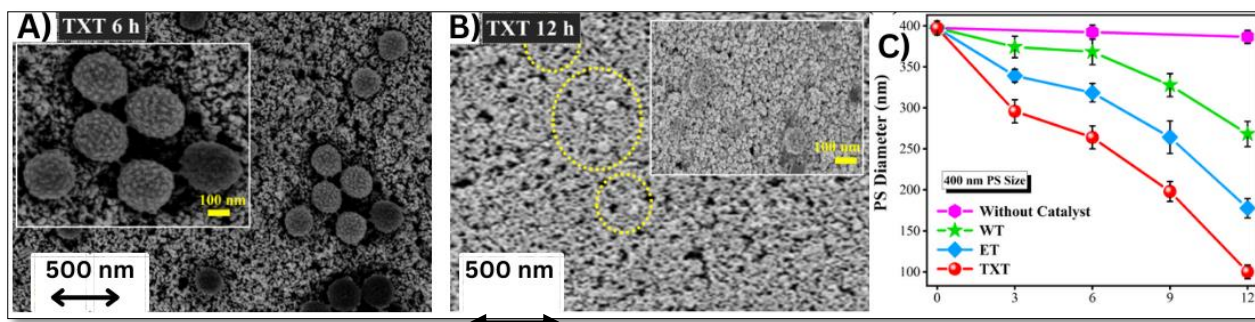


Figure 1.3: 'A' and 'B' showcases Triton X-100 based  $\text{TiO}_2$  after 6 hr irradiation and after 12 hr irradiation respectively. 'C' shows change in the diameter of a 400 nm PS, on TXT, Ethanol, Water films, and without catalyst with change in time of irradiation time. (Reproduced from Elsevier, *iScience*, 2020)

A way of enhancing photo-catalytic performance is doping.  $\text{TiO}_2$  is doped with metals to form 4% V- $\text{TiO}_2$ , Mn- $\text{TiO}_2$ , 0.4 Mo-doped  $\text{TiO}_2$ , W- $\text{TiO}_2$ . Using methods like absorption and co-precipitation. The catalyst was irradiated with UV light. Increase in the rutile content of the  $\text{TiO}_2$  pigment in the 4% polystyrene films results in decrease in the rate of degradation, bringing attention to the fact that the anatase-to-rutile ratio has a significant effect on the photo-catalytic behaviour of the pigment and that anatase is more photo-chemically active phase of titania. From figure 1.4 it's clearly visible that the highest rates of degradation are shown by the Mo- and W-doped anatase pigments as compared to rutile phase. There is decrease in the degradation rate of 4% V- $\text{TiO}_2$  when compared with the undoped  $\text{TiO}_2$  at the same calcination temperature. It is further seen that the degradation rate is inversely proportional to calcination temperature (figure 1.4). This concludes that the addition of vanadium lowers the rate of degradation. A similar trend is seen in the case of Mo- $\text{TiO}_2$ , the most aggressive pigments are 0.3 and 0.7% Mo-doped  $\text{TiO}_2$ , whereas 0.5% Mo-doped  $\text{TiO}_2$  and undoped  $\text{TiO}_2$  exhibit the slowest rates of degradation.<sup>29</sup>

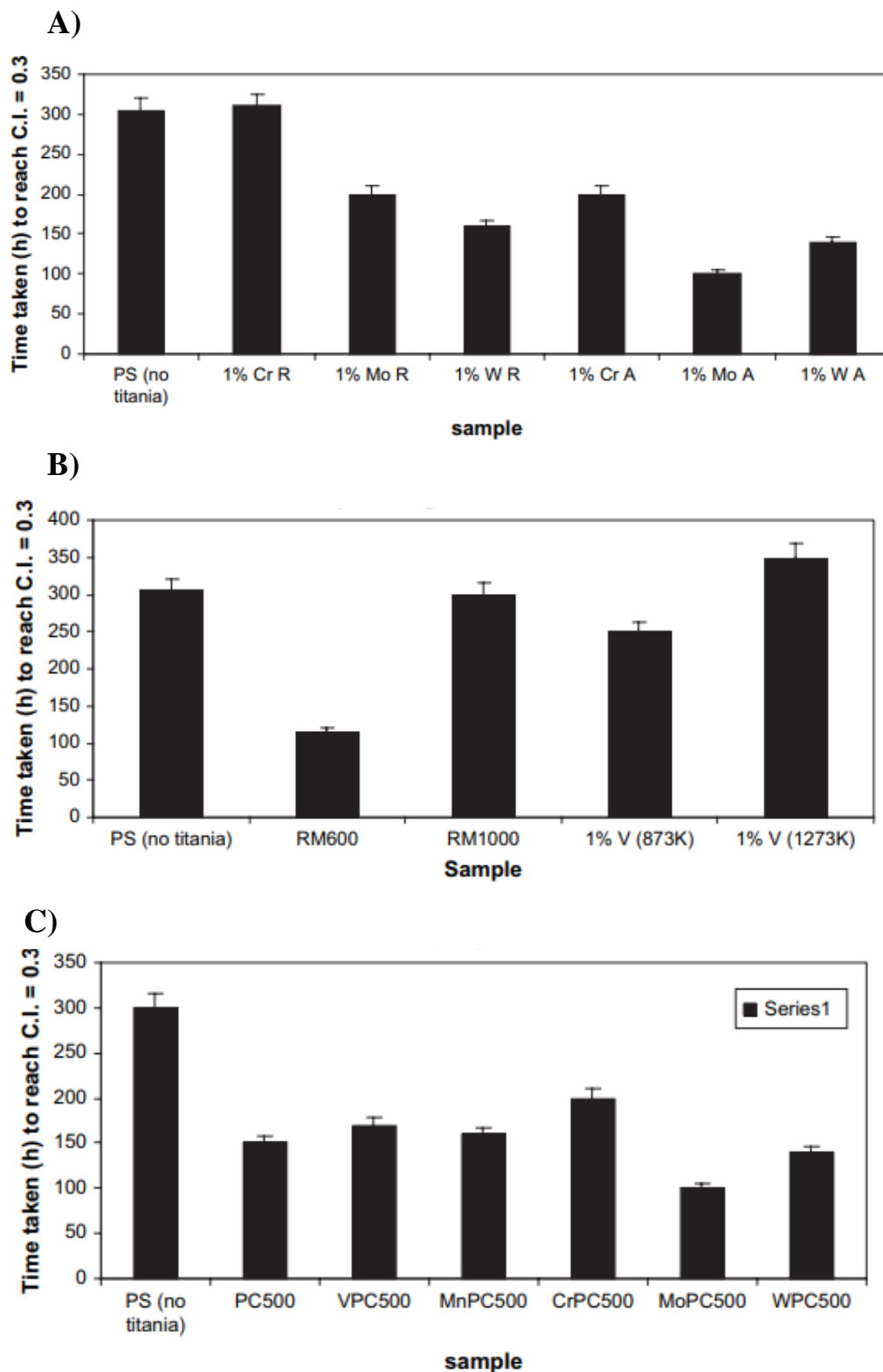


Figure 1.4: A-Graph depicts the effect of anatase and rutile phase on degradation of polystyrene, B- Graph depicts the effect of calcination temperature of V-doped  $\text{TiO}_2$  (co-precipitation method) [RM600 (20:80, anatase:rutile) and RM1000 (rutile)], C- The graph shows the time taken by group 6 metal-doped titania to reach carbonyl index of 0.3 after PS degradation. (Reproduced from Elsevier, ScienceDirect, 2006)

Micromotors are self-propelled nano-/microscale devices that are useful for micromotor's organic degradation, oil removal, and heavy metal removal. Photo-catalytic micromotors have many advantages such as immediate on/off switch, use of water as nontoxic fuel, and light as the renewable energy source. The light is easily controllable and does not lead to any waste products during the propulsion.  $\text{Au@mag@TiO}_2$ , mag = Ni, Fe, catalytic micromotor can move efficiently both in peroxide and water under UV light due to the photocatalytic reaction occurring on the particles.  $\text{Au@TiO}_2$  micromotors achieve very fast swimming speeds and therefore more pronounced phoretic phenomena, leading to a degradation efficiency of 67%. These micromotors using their efficient phoretic interactions and speed, transport and collect large amount of PS particles as seen from figure 1.5<sup>30</sup>.

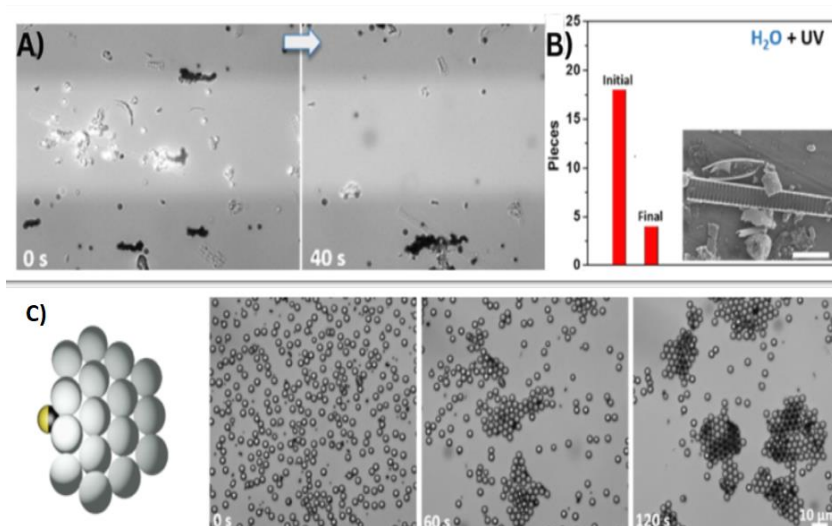


Figure 1.5: Micro-plastic sample from Warnow river in  $\text{H}_2\text{O}$  under 315 mW UV light (A). SEM images showcasing amount of PS microparticles in the initial and final states (B) (Scale bar: 10  $\mu\text{m}$ ), time-lapse optical images showcasing  $\text{Au@Ni@TiO}_2$  micromotors, collecting PS particles by phoretic interaction in 1.67%  $\text{H}_2\text{O}_2$  solution with 315 mW UV light (C). (Reproduced from Elsevier, *Journal of Hazardous Materials*, 2021)

### 1.2.3 Polyethylene terephthalate (PET)

Using PET at high temperatures can lead to the leaching of some toxic additives such as acetaldehyde, antimony and phthalates<sup>27</sup>.  $\text{N-TiO}_2$  was firstly synthesized by solvothermal and

calcination, and then  $\text{Bi}_2\text{O}_3$  nano-particles were loaded on its surface by wet-impregnation method and calcination. Bismuth oxide ( $\text{Bi}_2\text{O}_3$ ) is considered as a promising candidate to construct Z-scheme system with  $\text{TiO}_2$  due to its non toxicity, low cost, and appropriate band structure. The photo-catalytic performance of  $\text{Bi}_2\text{O}_3@\text{N-TiO}_2\text{-25\%}$  heterojunctions had been investigated preliminarily by decomposing the methyl orange (MO) solution under AM 1.5 irradiation. The photo-catalytic degradation efficiency of MO was up to 95.3% within 60 mins which is much higher than that of  $\text{N-TiO}_2$  and  $\text{Bi}_2\text{O}_3$ .  $\text{Bi}_2\text{O}_3@\text{NTiO}_2\text{-25\%}$  was compared with  $\text{N-TiO}_2$ , which indicates its excellent light-response capability. The heterojunction exhibited 40–50% total organic carbon (TOC) removal efficiency of various contaminants within 40 min, including MO, sodium dodecylbenzene sulfonate (SDBS), polyvinyl alcohol (PVA), dinotefuran (DTF), and tetracycline (TC). Therefore, it was concluded that the as-prepared  $\text{Bi}_2\text{O}_3@\text{N-TiO}_2\text{-25\%}$  heterojunctions possess excellent catalytic stability, reusability, and universality. Large amounts of debris were seen on the surface of PET-FMPs after being exposed for 48 h under AM 1.5 irradiation, with it showing a weight loss of  $2.21 \pm 0.99\%$  at pH 3. As seen in figure 1.7 at alkaline pH, 7, the weight loss was increased to  $10.23 \pm 1.91\%$  due to the production of oxidizing active species such as  $\cdot\text{OH}$ ,  $\cdot\text{O}_2^-$ ,  $^1\text{O}_2$ , and  $\text{h}^+$  in the alkaline media at room temperature and ambient pressure<sup>31</sup>. Another photo-catalyst with a surface area of  $115 \text{ m}^2/\text{g}$  and a band gap of approximately around 2.58 eV, synthesized by solvothermal method is  $\text{MXene}/\text{Z}_{0.6}\text{Cd}_{0.4}\text{S}$ . This degradation results in the evolution of hydrogen and formation of other molecules such as glycolate, acetate, ethanol, etc. Generally speaking  $\text{Zn}_x\text{Cd}_{1-x}$  become of interest due to its good optical properties, adjustable and appropriate band gap and high utilization rate of visible light along with this, it being a binary alloy of sulfides has higher capacity, chemical stability and electrochemical activity as compared to the single metal sulfides. In addition, MXene is reported to have a good Fermi level position and high electrical conductivity, which enables

it to act as an effective catalyst promoter to accelerate the separation of charge-hole, improving the photo-catalytic performance of the metal sulphides. It is observed that the hydrogen and evolution decreases with increase in MXene concentration. Because the excessive load of MXene effectively might block the absorption of visible light, therefore an appropriate MXene loading amount is required to enhance the photo-catalytic H<sub>2</sub> evolution activity as seen in figure 1.6. The experimental results showcased M-2/Z<sub>0.6</sub>C<sub>0.4</sub>S is the highest, which is 14.17 mmol/hg . This is due to the synergistic effect of improved charge-hole separation efficiency, increased visible light absorption capacity and appropriate oxidation potential.

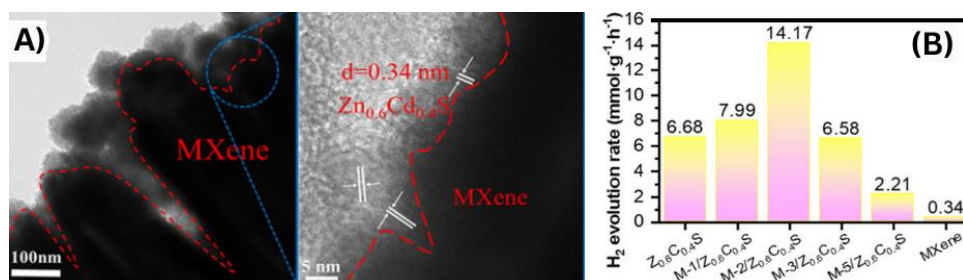


Figure 1.6: ‘A’ represents HRTEM of MXene/Z<sub>0.6</sub>C<sub>0.4</sub>S, ‘B’ represents Photocatalytic H<sub>2</sub> evolution over MXene/Z<sub>x</sub>C<sub>1-x</sub> (Reproduced from Elsevier, *Journal of Colloid and Interface Science*, 2022)

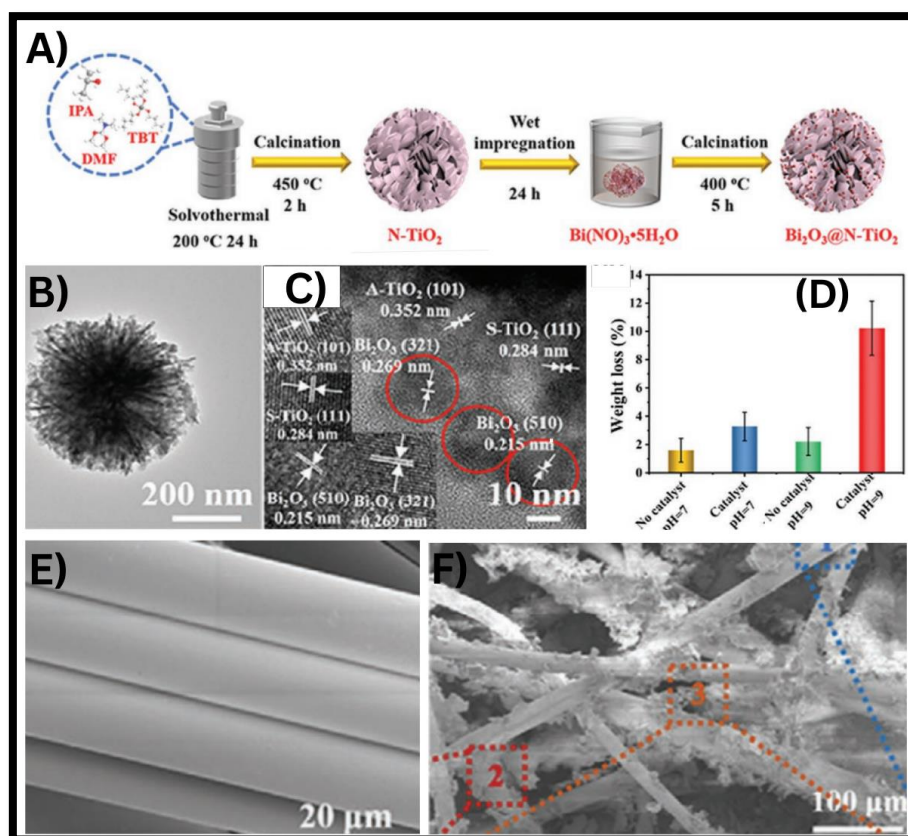


Figure 1.7: Solvochemical preparation process of the  $\text{Bi}_2\text{O}_3@\text{N-TiO}_2$  (A), TEM image of nanoflower-like structure of  $\text{Bi}_2\text{O}_3@\text{N-TiO}_2$  (B), The HRTEM image of  $\text{Bi}_2\text{O}_3@\text{N-TiO}_2$  (C), plot representing the Weight loss of polyethylene terephthalate (PET)-FMPs after photocatalytic degradation at different pH = 7,9 and with presence and absence of  $\text{Bi}_2\text{O}_3@\text{N-TiO}_2$ -25% (D), SEM image of PET-FMPs and PET-FMPs with  $\text{Bi}_2\text{O}_3@\text{N-TiO}_2$ -25% added after photocatalytic degradation under AM 1.5 irradiation at pH = 9 (E-F).

(Reproduced from ScienceDirect, Advanced Sustainable Systems, 2022)

### 1.2.4 Polypropylene

Polypropylene is used in the packaging of medicines, beverages etc due to its strong and semi-transparent properties. Unlike polyethylene, polypropylene is not harmful to humans. Polypropylene films with  $\text{TiO}_2$  nano-particles incorporated are studied with xenon lamps used as the radiation source. The precursor  $\text{TiO}_2$  powder is prepared using sol gel method and it should have crystalline structure of anatase to yield better results. Its morphology is visible in figure 1.8 .The polypropylene film incorporated with  $\text{TiO}_2$  nano-particles formed with calcinations at  $500^\circ\text{C}$  showed surface area of  $74 \text{ m}^2/\text{g}$  and pore size of 8 nm. It had the band

gap of about 3.28 eV. The average weight of films was around 0.0759 g and the thickness of films tested was of around 0.102 mm. Before irradiation all films of polymer with different concentrations of TiO<sub>2</sub> were translucent. As films containing photo-catalysts were irradiated its colour turned white. A degradation efficiency of 4 to 8 % was shown with the final products formation<sup>32</sup>.

Another way to enhance the degradation of micro-plastics is by synthesizing Polypropylene film with C-TiO<sub>2</sub> nano-particles. To maintain control over the photo-catalytic properties one can attempt to coat TiO<sub>2</sub> with carbon layer. Studies have shown that the photo-catalytic properties of carbon coated TiO<sub>2</sub> depend on the thickness of the layer. It is reported that the carbon coating suppresses the anatase to rutile phase transformation that is advantageous to photodecomposition of organic material, but once the threshold is crossed thicker the carbon layer becomes, weaker is the ability of UV rays to penetrate. This consequently reduces the photo-catalytic property. Hence the photo-catalytic property will be decreased if the depth of the carbon layer is too thick; hence it is necessary to find the right balance of carbon layer thickness. Another important factor is the particle size. It has been agreed upon that the degradation process begins from the interface between the Polypropylene and TiO<sub>2</sub> and then extends outwards to the inner film while spreading over the film surface simultaneously. Particle size and the interface area between the PP and TiO<sub>2</sub> are inversely proportional. Therefore in this case, the photodegradation efficiency of the composite film will decrease with light irradiation from 75-W UV lamp (254 nm) for 100-500 hours<sup>33</sup>.

ZnO nano-particles, with a band gap of 3.37 eV, have been used for catalytic degradation of 25 mm<sup>2</sup> polypropylene films under UV light in an aqueous medium. It is seen that the influence of plastic size affects polypropylene decomposition, it is more prominent at high temperature, hence the combination of high reaction temperature (50 ° C), 1 g/L ZnO and low size of PP plastic (25 mm<sup>2</sup>) resulted in high PP weight loss that is 7.89%<sup>34</sup>. zinc oxide

nanorods immobilized onto glass fibers substrates(diameter  $\sim 16\mu\text{m}$ ) were synthesized hydrothermally. The idea was to induce photo-catalytic degradation of Polypropylene micro-plastics spherical particles suspended in water by irradiation of zinc oxide nanorods (ZnO NRs) immobilized onto glass fibers substrates in a flow through system,. Exposure of 2 weeks in visible light reduced the particle volume by 65%. The surface area of a typical  $2\mu\text{m}$  ZnO NR is calculated to be  $\sim 1.5 \times 10^3 \text{ nm}^2$ . This process resulted in the formation of ethynyloxy/acetyl radicals, hydroxypropyl, butyraldehyde, acetone, acrolein (propenal) and pentyl group etc <sup>35</sup>

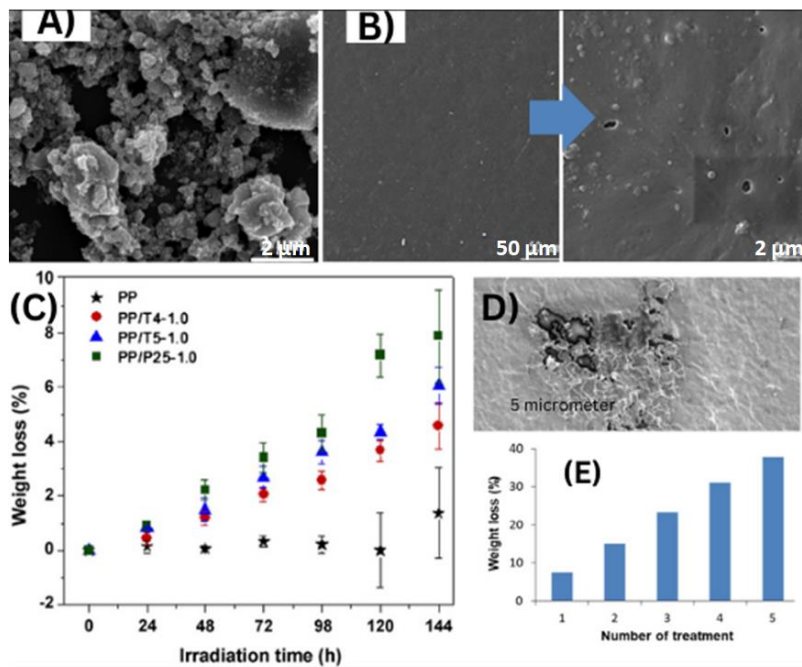


Figure 1.8: A)SEM images of TiO<sub>2</sub> synthesized using sol-gel method after a thermal treatment at 500°C, B)SEM images of pure PP and PPDTi (97.9 pp %W of type P25 with 2% W TiO<sub>2</sub> and 0.1 % W antioxidant) after 100 hr UV radiation, C) Evolution of weight of TiO<sub>2</sub>/polypropylene films at different irradiation times. D) PP plastic treated using 1 g/L ZnO at 50°C E) plastic weight loss with increase in number of thermo-photocatalytic treatment cycle. (Reproduced from Elsevier, Materials Research Bulletin ,2014)

### 1.2.5 High Density Polyethylene (HDPE)

HDPE is synthesized using petroleum and is produced at a massive scale due to its heat resistant quality and the absence of phthalates or even BPA<sup>27</sup>. N-Doped TiO<sub>2</sub> was used as the photo-catalyst in the degradation process of these micro-plastics. 2 methods of synthesis were used for N-TiO<sub>2</sub>, one was the normal sol-gel method while other was synthesizing from mussel proteins. Photodegradation test was carried out at room temperature for around 20 hours, with about 50% humidity. It was observed that the catalyst prepared using sol gel method showed higher crystallinity. From SEM images it was observed that the protein derived TiO<sub>2</sub> showed higher porosity it also showed band gap of 2.9 eV as compared to sol gel synthesized TiO<sub>2</sub> (3.1 eV). As mentioned earlier humidity is an important condition for these reactions, providing hydroxide radicals for photodegradation to occur<sup>36</sup>. N-TiO<sub>2</sub> was also synthesized using evaporation-induced self-assembly (EISA) method which similar to sol gel method showed 3.1 eV band gap. The pore size was observed to be 10 nm, with a surface area of  $74.7 \pm 0.2 \text{ m}^2/\text{g}$ . When irradiated with visible light mass loss of 4.65% was observed. In the figure below you can see the biggest HDPE\_A MPs, the blue curve shows that mass loss after 50 h of irradiation was very limited, with a mean value of 0.22% (0.02 SE). This result was explained by the intrinsic characteristics of the MPs. HDPE was not soluble in the reaction medium, and the particle size of this sample was huge compared with the particles or pores of N-TiO<sub>2</sub> ( $67.8 \times 10^3$  times larger). These characteristics prevented the adsorption of the micro-plastic explaining their limited mass loss. In the case of HDPE MPs derived from Scrub B, they were  $31.8 \times 10^3$  times larger than N-TiO<sub>2</sub> particles, and adsorption of these plastics on the semiconductor surface was not possible.<sup>23</sup>.

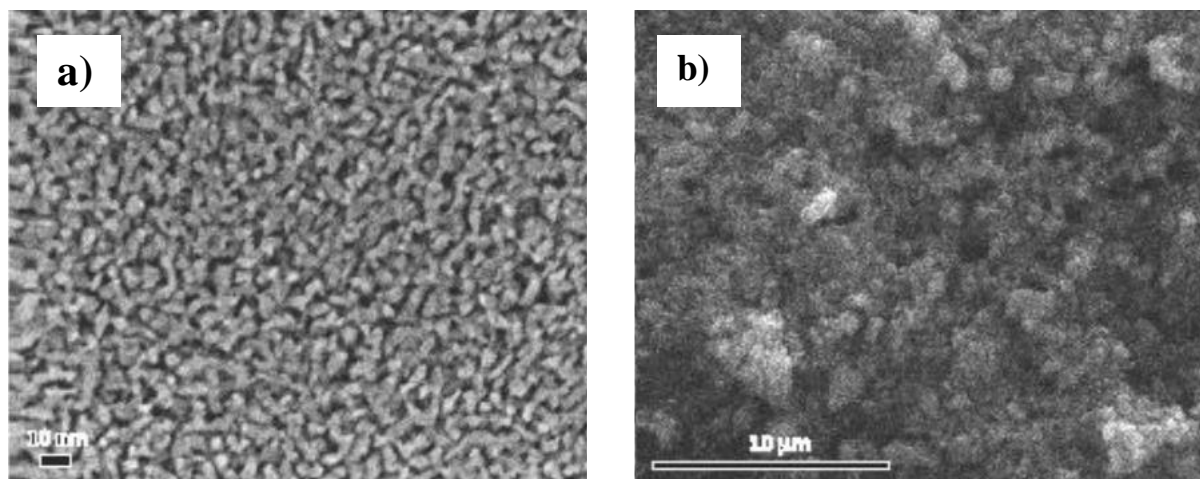


Figure 1.85: FE-SEM micrographs of the (a) sol-gel and (b) protein-derived N-TiO<sub>2</sub> semiconductors (*Reproduced from Ceramics international, 2019*)

### 1.2.6 Polyethylene

TiO<sub>2</sub> nano-particles are widely used photo-catalyst used in polyethylene photo-catalytic degradation under UV light. The process results in the production of carbon dioxide, water and carbon monoxide. With the use of raman spectroscopy it was observed that with the increase in the irradiation time the morphology of polyethylene was changing, finally After irradiation of 36 hours, complete degradation was seen<sup>28</sup>. It was also observed that modifying the TiO<sub>2</sub> with silver and reduced graphene oxide was increasing the degradation efficiency. The degradation efficiency of 3% Ag/TiO<sub>2</sub> was found to be 68%, with a band gap of 2.85 eV, while that of 3% Ag/TiO<sub>2</sub>-1%-RGO was found to be 76% as compared to TiO<sub>2</sub> which showed band gap of 3.2 eV. This increase in the degradation efficiencies can be due to many reasons such as the dopant added is a good electron trapper decreasing the energy gap between conduction band and valence band, making it able to absorb visible light. This coupled with plasmonic effect increase the electron-hole charge separation. When 3% Ag/TiO<sub>2</sub> was doped with 1 % RGO it enhance the degradation efficiency further this can be attributed to reduced graphene oxides ability to increase the mobility of the electrons. RGO has large surface area

which ensures better access for catalysts to the pollutants<sup>37</sup>. Photo-catalyst, BiOCl-X was used for degrading polyethylene under visible light. The presence of hydroxyl groups on the surface of the catalyst was beneficial to promote further formation of  $\cdot\text{OH}$  making it an ideal choice to study photo-catalytic degradation. BiOCl-1 showed higher hydroxyl group richness than BiOCl with the band gap of 3.29 eV as compared to 3.39 eV<sup>36</sup>. Table 1 shows the reduction of mass of micro-plastic with time in the presence of various catalysts.

Table 1: Micro-plastic mass reduction of polyethylene

| Catalyst                           | Micro-plastic mass reduction       |      |      |      |      |
|------------------------------------|------------------------------------|------|------|------|------|
|                                    | Mass of micro-plastic (mg) at time |      |      |      |      |
|                                    | 0 hr                               | 1 hr | 2 hr | 3 hr | 4 hr |
| Without catalyst                   | 50                                 | 50   | 50   | 50   | 50   |
| TiO <sub>2</sub> P25               | 50                                 | 40   | 32   | 26   | 22   |
| 3% Ag/TiO <sub>2</sub>             | 50                                 | 30   | 24   | 19   | 16   |
| 3% Ag/TiO <sub>2</sub> -<br>1% RGO | 50                                 | 28   | 18   | 14   | 12   |

Table 1.1: Photo-catalysts used in micro-plastic degradation

| SR. NO | Citations     | Photo-catalyst and morphology                                        | Method of Synthesis            | Surface area m <sup>2</sup> /g       | Por e size(d) | Band gap       | Contami nant                                                                       | Source                                                | Degradation efficiency                  | Products formed                                                                                       |
|--------|---------------|----------------------------------------------------------------------|--------------------------------|--------------------------------------|---------------|----------------|------------------------------------------------------------------------------------|-------------------------------------------------------|-----------------------------------------|-------------------------------------------------------------------------------------------------------|
| 1      | <sup>21</sup> | ZnO (Nanorods)                                                       | Hydrothermal process           | 55 cm <sup>2</sup>                   |               |                | low-density polyethylene (LDPE) film                                               | Visible light                                         | Carbonyl index:1.51<br>Vinyl index:1.3  | CO <sub>2</sub> ; H <sub>2</sub> O                                                                    |
| 2      | <sup>24</sup> | (ZnO-Pt) (nanorods)                                                  | UV-C photoreduction method     | -                                    |               |                | Methylene blue , low-density polyethylene (LDPE) film                              | Visible light                                         | Carbonyl index:1.49<br>Vinyl index:1.35 | -                                                                                                     |
| 3      | <sup>34</sup> | ZnO nanoparticles                                                    | -                              |                                      | -             | 3.37           | polypropylene plastic                                                              | UV light                                              | 7.8 wt% (at 50°C)                       |                                                                                                       |
| 4      | <sup>35</sup> | zinc oxide nanorods immobilized onto glass fibers                    | Hydrothermal method            | 1.5 *10 <sup>3</sup> nm <sup>2</sup> |               | -              | PolyPropylene micro-plastics spherical particles                                   | Visible light a tungsten-halogen lamp of 120 W(456hr) | Reduction of average volume by 65%      | ethynyl/ acetyl radicals, hydroxypropyl, butyraldehyde, acetone, acrolein (propenal) and pentyl group |
| 5      | <sup>38</sup> | M-2/Zn <sub>0.6</sub> Cd <sub>0.4</sub> S (accordion-like structure) | Solvothermal method            | 115                                  |               | Approx 2.58 eV | polyethylene terephthalate (PET)                                                   | Visible light (>420 nm) 300 W Xenon lamp              |                                         | H <sub>2</sub> evolution glycolate, acetate, ethanol, etc                                             |
| 6      | <sup>29</sup> | 4% V-TiO <sub>2</sub>                                                | absorption and coprecipitation | -                                    | -             | -              | Polystyrene                                                                        | UV light                                              | -                                       | -                                                                                                     |
| 7      | <sup>32</sup> | TiO <sub>2</sub> nanoparticles                                       | sol-gel method                 | 74                                   | 8 nm          | 3.28 eV        | Polypropylene with an average molecular weight (Mw) of 380,000 g mol <sup>-1</sup> | Xenon lamps as irradiation source (1800 W)            | -                                       | CO <sub>2</sub> ; H <sub>2</sub> O                                                                    |

|    |               |                                                                                                         |                                                                         |            |            |                                                               |                                                          |                                                  |                                                                                                               |                                                 |
|----|---------------|---------------------------------------------------------------------------------------------------------|-------------------------------------------------------------------------|------------|------------|---------------------------------------------------------------|----------------------------------------------------------|--------------------------------------------------|---------------------------------------------------------------------------------------------------------------|-------------------------------------------------|
| 8  | <sup>33</sup> | C-TiO <sub>2</sub> (Nanoparticles)                                                                      | -                                                                       | -          | -          | -                                                             | PolyPropylene nanocomposite                              | 75-W UV lamp                                     | 78%                                                                                                           | -                                               |
| 9  | <sup>22</sup> | TiO <sub>2</sub> nano tubes                                                                             | Hydrothermal method                                                     | 161        |            |                                                               | Polyethylene films (LDPE films)                          | UV radiation                                     | 67% .                                                                                                         |                                                 |
| 10 | <sup>22</sup> | TiO <sub>2</sub> (nanoparticles)                                                                        |                                                                         | 81         | -          | -                                                             | Polyethylene films (LDPE films)                          | UV radiation                                     | Mass loss: 6.40%                                                                                              | -                                               |
| 11 | <sup>36</sup> | 1. N-TiO <sub>2</sub> film (agglomerated particles)<br><br>2. mussel-derived N-TiO <sub>2</sub> powders | sol-gel synthesis<br><br>green synthesis                                |            |            | 3.1 eV (400 nm)<br><br>Higher porosity<br><br>2.9 eV (427 nm) | HDPE microplastics                                       | visible light                                    | 67%                                                                                                           |                                                 |
| 12 | <sup>30</sup> | Au@Ni@TiO <sub>2</sub> Micromotors (700 nm)                                                             | hydrolysis and condensation reaction of TTIP(Titanium(IV) isopropoxide) | -          | -          | -                                                             | Polystyrene MPs                                          | UV light 315 W Colibri lamp( $\lambda$ = 385 nm) | 1.98.40 % of 400 nm PS (12hr)<br><br>2. tens of micrometers sized PE showed complete degradation after 36 hrs | -                                               |
| 13 | <sup>28</sup> | TiO <sub>2</sub> nanoparticle                                                                           | -<br><br>-                                                              | -<br><br>- | -<br><br>- | -<br><br>-                                                    | 1. polystyrene microspheres (PS)<br>2. polyethylene (PE) | UV light (50 hr)                                 | Mass loss of 0.22%<br><br>Mass loss of 4.65%                                                                  | -<br><br>CO <sub>2</sub> , H <sub>2</sub> O, CO |

|    |               |                                                                                                                                   |                                                                                         |                                      |                            |                                            |                                                                        |                                                  |                                                  |                                                       |
|----|---------------|-----------------------------------------------------------------------------------------------------------------------------------|-----------------------------------------------------------------------------------------|--------------------------------------|----------------------------|--------------------------------------------|------------------------------------------------------------------------|--------------------------------------------------|--------------------------------------------------|-------------------------------------------------------|
| 14 | <sup>39</sup> | N-TiO <sub>2</sub> coating (nano-particles)                                                                                       | evaporation-induced self-assembly (EISA) method                                         | 74.7 ± 0.2                           | 10 nm                      | 3.1 eV                                     | Spherical primary HDPE MPs<br><br>film-shaped secondary LDPE MPs       | Visible light 50 W Visible LED Lamp              | 12.42 ± 0.20 %                                   | inert products such as alkenes, aldehydes and ketones |
| 15 | <sup>23</sup> | carbon and nitrogen-doped TiO <sub>2</sub> (nano-particles)                                                                       |                                                                                         | 219.42 ± 1.82                        | 0.85 ± 0.36 μm of diameter | 2.9 eV                                     | HDPE MPs                                                               | Visible light (428 nm)                           | 56%<br>68%<br>76%                                |                                                       |
| 16 | <sup>37</sup> | TiO <sub>2</sub><br><br>3% Ag/TiO <sub>2</sub><br><br>Ag/TiO <sub>2</sub> /RGO Reduced Graphene oxide (RGO) (Spherical particles) | Photo-assisted Deposition<br><br>Co-precipitation                                       |                                      |                            | 3.2 eV<br><br>2.85 eV                      | polyethylene scrub sized 100-150 micrometer                            | UV radiation for 4 hours                         | 10.23 ± 1.91 wt% of polyethylene terephthalate ( |                                                       |
| 17 | <sup>31</sup> | Bi <sub>2</sub> O <sub>3</sub> @N-TiO <sub>2</sub> – 25% heterojunction (nanoflower like structure)                               | 1. Solvothermal method, calcination<br><br>2. wet-impregnation strategy and calcination | -                                    | -                          | 2.84 eV                                    | Polyethylene Terephthalate Fiber-Based Microplastics in Alkaline Media | AM 1.5 irradiation for 48 hours                  | 5.38%                                            |                                                       |
| 18 | <sup>39</sup> | BiOCl-X (platform nanosheets)                                                                                                     | Co-precipitation                                                                        | 52.00 (BiOCl-1)<br><br>17.97 (BiOCl) |                            | 3.39 (BiOCl)<br>eV<br>3.29 (BiOCl-1)<br>eV | Polyethylene MPs                                                       | Visible light 250 W Xe lamp (λ > 420 nm)         | weight loss is 10%<br><br>weight loss is 12.5 %  |                                                       |
| 19 | <sup>25</sup> | Polyacrylamide-grafted ZnO nano-particles (                                                                                       | Ultrasonication method                                                                  |                                      |                            |                                            | LDPE (polyethylene)                                                    | UV light Lamps with a power of 30 W (350–280 nm) |                                                  | CO <sub>2</sub> ; H <sub>2</sub> O                    |

This literature survey summarises the various metal oxides used in the photocatalytic degradation of micro-plastics. It is observed that  $\text{TiO}_2$  nano tubes possessing an average size of 40 nm shows highest degradation efficiency of 78% of LDPE micro-plastic under UV irradiation. Attempts to carry out degradation within visible region by dye sensitization lowered the efficiency to 48% ,after irradiation was carried out for 4 to 5 days .Whereas  $\text{Ag/TiO}_2/\text{RGO}$  (Reduced Graphene oxide) degraded polyethylene with an efficiency of 76% under UV irradiation. Zinc oxide nanorods immobilized onto glass fibers (diameter  $\sim 16\mu\text{m}$ ) substrates showed average 65% reduction in volume of polypropylene film under visible light after irradiation for 456 hours. It was observed that  $\text{MXene}/\text{Z}_{0.6}\text{Cd}_{0.4}\text{S}$  had a band gap of 2.58 eV when compared with  $\text{Bi}_2\text{O}_3@\text{N-TiO}_2 - 25\%$  heterojunction with a band gap of 2.84 eV in the degradation of PET. Hydrothermal method was seen to synthesize better photocatalysts as compared to other methods. Even with the efficiency of the above mentioned catalysts we still need to find a more affordable and efficient method for micro-plastic degradation such as using  $\text{MnCo}_2\text{O}_4$  and  $\text{CuCo}_2\text{O}_4$  to photo-catalytically degrade micro-plastics as mentioned in the above section 2.2.

### 1.2.7 Methylene Blue as water pollutant

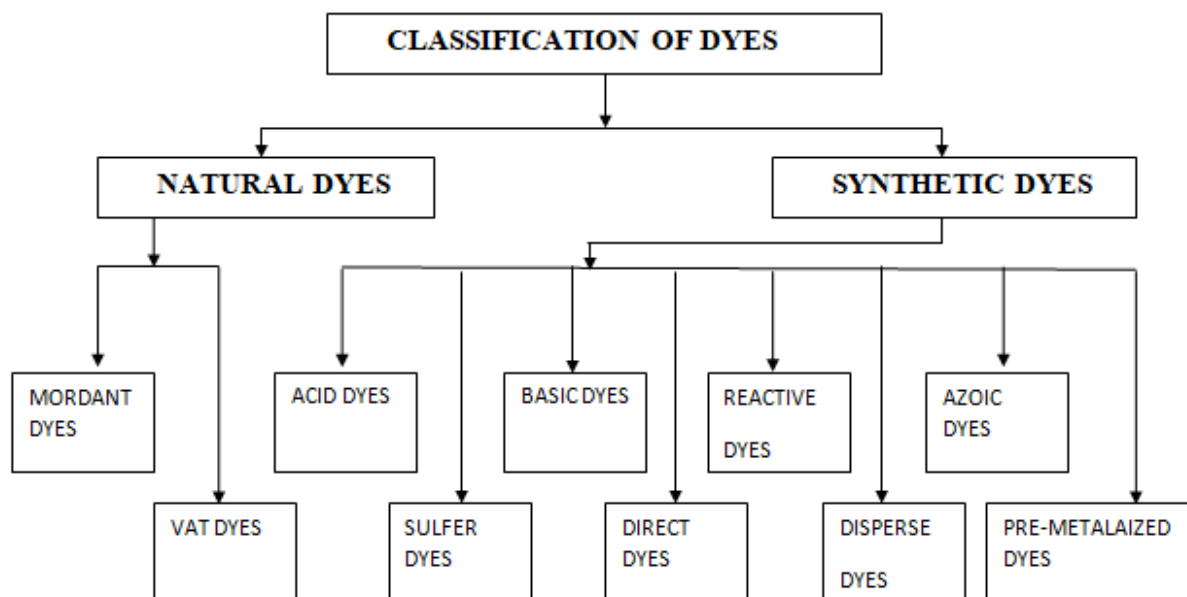


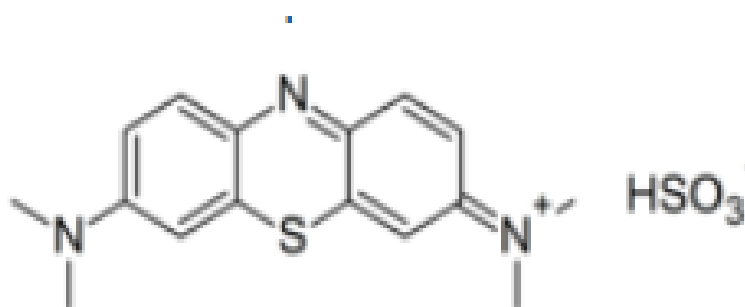
Figure 1.90: Classification of Dyes

Natural dyes are derived without the use of chemicals from minerals, plants, and animals. A few of its benefits include colour variety, ease of disposal, and biodegradability. But they also have drawbacks, such as a lack of colour availability, subpar colour yield, a difficult dyeing procedure, subpar fastness qualities, and a tough time combining dyes. Synthetic dyes are those made from either organic or inorganic compounds. They are chosen over natural dyes because they are less expensive, offer a wide variety of hues, and give the materials they dye greater qualities.

Before the invention of a mordant or employing agent, basic dyes were employed to colour wool, silk, linen, hemp, and other fabrics. On cotton and rayon, they were employed with a mordant like tannic acid. Basic dyes offer acrylic fibres vivid colours with outstanding fastness. They can be applied to basic nylon and polyester dyeable varieties. "Cationic dyes" is another name for these colours. Cationic dyes are those that in an aqueous solution can separate into positively charged ions. They can interact with the fiber's negative group to

create a salt, which is then firmly bonded to the fibre and used to colour it. These colours are typically applied combined with organic acids and hydrochlorides of organic bases.

Methyl thioninium chloride, often known as methylene blue (MB), is a tricyclic phenothiazine that is soluble in water and some organic solvents. Over the years, it has been utilised as a treatment for illnesses such as methemoglobinemia and malaria. It is sprayed into the mucosa of the digestive system during chromoendoscopy as a dye to detect dysplasia or pre-cancerous lesions. It is a synthetic dye that is frequently used for colouring leather, papers, and fabrics in the garment and textile industries. It has a long history of application in analytical chemistry as a redox indicator. When in an oxidising environment, this substance's solutions are blue; nevertheless, when exposed to a reducing agent, they become colourless.



A significant amount of wastewater containing the dye methylene blue is released into water bodies as industrialization grows. The monoamine oxidase inhibiting properties of MB dye, which can cause lethal serotonin poisoning in humans at concentrations higher than 5 mg/kg, also pose a serious threat to the aquatic ecosystems fauna. Therefore, it is crucial to remove MB dye from wastewaters. Therefore, before disposal, it is crucial to treat methylene blue waste water<sup>40</sup>.

## **OBJECTIVES**

Since it is observed that the ternary metal cobalt oxides of manganese and copper have not been widely investigated in the field of micro-plastic degradation. My objective is:

1. To determine the efficiency of photo-catalytic degradation of micro-plastic and methylene blue using  $\text{MnCo}_2\text{O}_4$  and  $\text{CuCo}_2\text{O}_4$  as the photo-catalysts.
2. To investigate photo-catalytic degradation of micro-plastic such as LDPE.
3. To learn various synthesis and characterization techniques for fabrication of semiconductor nano-catalysts.

# CHAPTER II

## **2.0 Prologue**

This chapter discusses the various approaches taken to synthesize mixed metal cobaltites. Coprecipitation synthesis of  $MnCo_2O_4$  is discussed using different structure directing agents/SDAs (Urea, Thiourea, Semicarbazide, Thiosemicarbazide), at pH 9.

## **2.1 Materials used**

Cobalt acetate tetrahydrate (99%, Spectrochem PVT.LTD), Manganese acetate tetrahydrate (99%, Loba chemie), Semicarbazide hydrochloride (98%, Thomas Baker (Chemicals) PVT.Limited), Urea (99%, Molychem), Cupric acetate monohydrate (99%, SDFCL), Sodium carbonate (99.9%, Thomas baker), methylene blue, LDPE (Thermo Fischer Scientific)

## **2.2 Protocols for co-precipitation synthesis of $MCo_2O_4$ (M= Mn, Cu)**

### **• 2.2.1 Pristine condition**

In the synthesis of  $MCo_2O_4$  (M= Mn, Cu), cobalt acetate hexahydrate,  $(CH_3COO)_2Co \cdot 6H_2O$  and metal acetates were weighed as mentioned in table 5 and they were dissolved in minimum amount of water are mentioned in appendix I section. The cobalt-metal solution was placed on the magnetic stirrer with temperature between 30–40°C. pH adjustment was done using 1 M sodium carbonate. The solution was kept for 2 hr continuous stirring and then filtered. The washings were done with double distilled water. The precipitate was air dried and calcined at 550 °C for 3 hours. The compound obtained was weighed. The yield of  $MCo_2O_4$  (M=Mn, Fe, Ni, Cu), formed is recorded in table 2.5.

- **2.2.2 Using structure directing agents**

In the synthesis of  $M\text{Co}_2\text{O}_4$  ( $M = \text{Mn, Cu}$ ), cobalt acetate hexahydrate,  $(\text{CH}_3\text{COO})_2\text{Co}\cdot 6\text{H}_2\text{O}$  and metal acetates were weighed as mentioned in table 1.2 and they were dissolved in minimum amount of water. The SDAs were weighed (stoichiometric ratio 1:2) as mentioned in table 1.2 and diluted in minimum amount of distilled water as well. The weights for the precursors and SDAs were calculated and are mentioned in appendix I section. The cobalt-metal solution was placed on the magnetic stirrer with temperature between 30–40°C. The prepared SDA solutions were added drop wise, followed by pH adjustment using 1 M sodium carbonate. The solution was kept for 2 hr continuous stirring and then filtered. The washings were done with double distilled water. The precipitate was air dried and calcined at 550 °C for 3 hours. The compound obtained was weighed. The yield of  $M\text{Co}_2\text{O}_4$  ( $M = \text{Mn, Cu}$ ), formed is recorded in table 1.3.

Table 1.2: Amount of SDA's and precursors added for the synthesis of  $M\text{Co}_2\text{O}_4$  ( $M = \text{Mn, Cu}$ )

| Sr. No. | SDA           | Amount of $\text{Mn}(\text{CH}_3\text{COO})_2\cdot 4\text{H}_2\text{O}$ weighed (g) | Amount of $\text{Co}(\text{CH}_3\text{COO})_2\cdot 4\text{H}_2\text{O}$ weighed (g) | Amount of SDA Weighed (g) |
|---------|---------------|-------------------------------------------------------------------------------------|-------------------------------------------------------------------------------------|---------------------------|
| 1.      | Pristine      | 1.55                                                                                | 3.15                                                                                | -                         |
| 2.      | Urea          |                                                                                     |                                                                                     | 2.276                     |
| 3.      | Semicarbazide |                                                                                     |                                                                                     | 4.28                      |

| Sr. No. | SDA           | Amount of $\text{C}_4\text{H}_6\text{CuO}_4\cdot \text{H}_2\text{O}$ Weighed (g) | Amount of $\text{Co}(\text{CH}_3\text{COO})_2\cdot 4\text{H}_2\text{O}$ Weighed (g) | Amount of SDA Weighed (g) |
|---------|---------------|----------------------------------------------------------------------------------|-------------------------------------------------------------------------------------|---------------------------|
| 1.      | Pristine      | 1.22                                                                             | 3.048                                                                               | -                         |
| 2.      | Urea          |                                                                                  |                                                                                     | 2.2034                    |
| 3.      | Semicarbazide |                                                                                  |                                                                                     | 4.082                     |

Table 1.3: Yield of  $M\text{Co}_2\text{O}_4$  (M= Mn,Cu) at ~9 pH in the presence of various structure directing agents.

| Sr.No. | Compound                         | SDA           | Weight of as-synthesised compound (g) | Weight of calcined oxides (g) | Yield (%) |
|--------|----------------------------------|---------------|---------------------------------------|-------------------------------|-----------|
| 1      | MnCo <sub>2</sub> O <sub>4</sub> | Pristine      | 0.9827                                | 0.5663                        | 37.7      |
| 2      |                                  | Urea          | 2.4382                                | 1.3497                        | 89.98     |
| 4      |                                  | Semicarbazide | 0.9097                                | 0.3497                        | 23.31     |
| 6      | CuCo <sub>2</sub> O <sub>4</sub> | Pristine      | 4.1497                                | 0.622                         | 41.47     |
| 7      |                                  | Urea          | 5.81                                  | 1.2876                        | 85.84     |
| 9      |                                  | Semicarbazide | 0.5146                                | 0.1089                        | 7.26      |

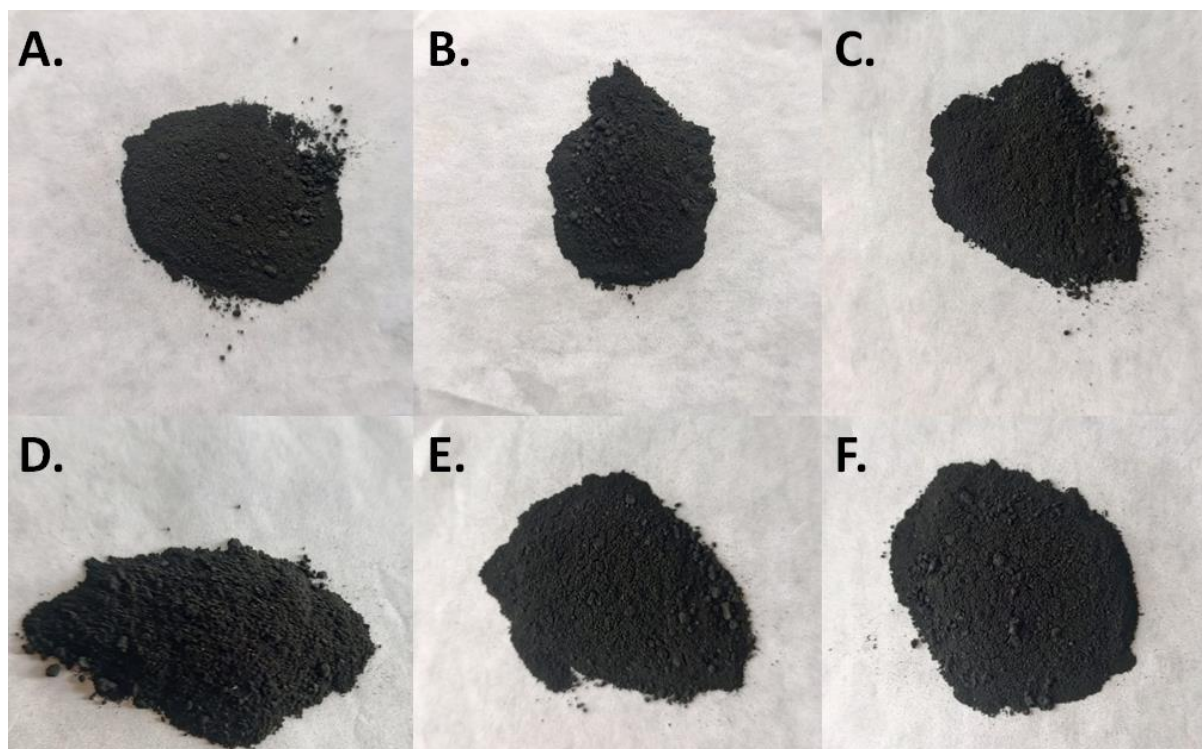


Figure 2.0:  $M\text{Co}_2\text{O}_4$  (M=Cu, Mn) compounds in pristine conditions (A, B), also using urea(C, D) semicarbazide (E,F) SDAs

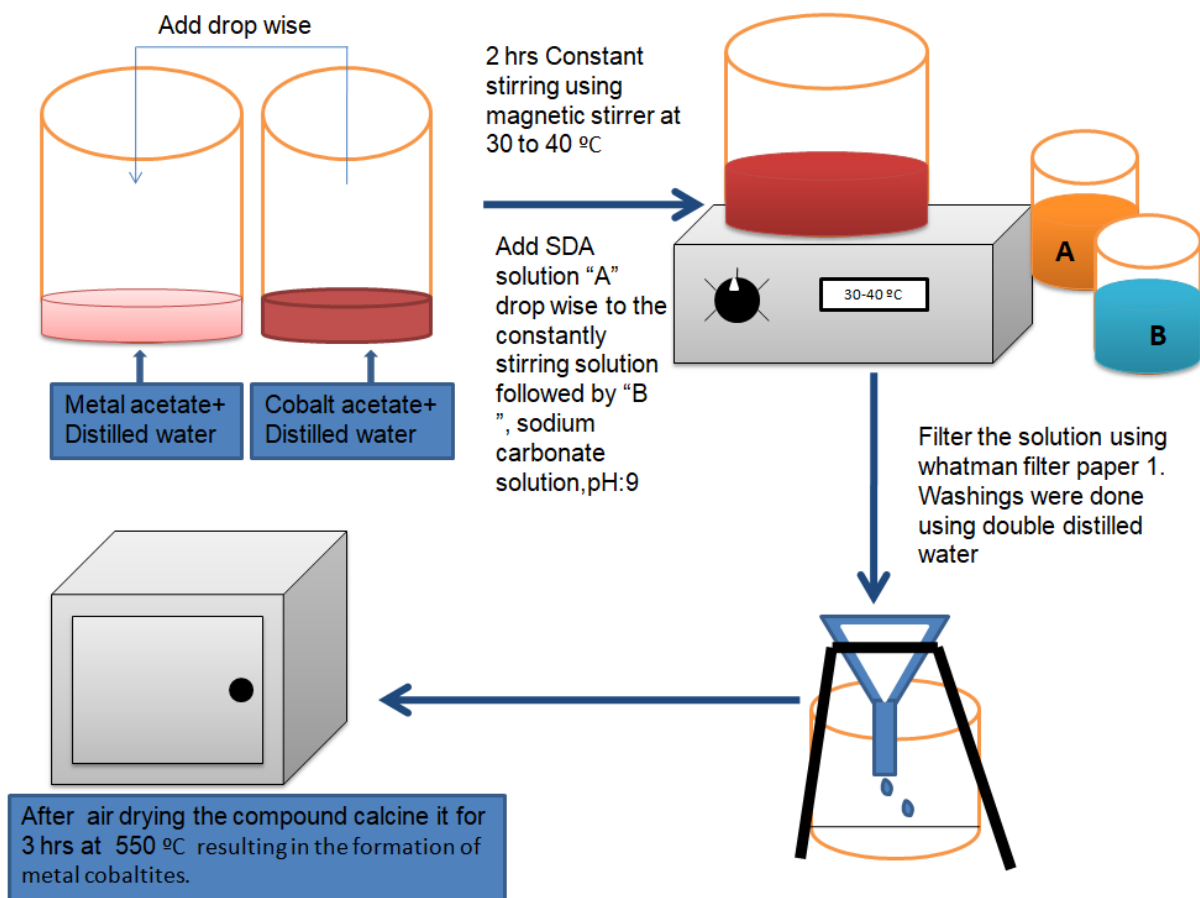


Figure 2.1: Schematic representing synthesis process of  $MCo_2O_4$  ( $M=Cu, Mn$ ) compounds in pristine conditions, also using urea and semicarbazide SDAs

# CHAPTER III

### **3.0 Prologue**

The following chapter talks about various instruments used for characterization of synthesized compounds. It also discusses the data obtained from characterization of  $\text{MnCo}_2\text{O}_4$  using FTIR, SEM, Elemental analysis, XRD and UV-DRS.

### **3.1 Instrumentation**

The characterization of the Manganese Cobaltite,  $\text{MnCo}_2\text{O}_4$  prepared by co-precipitation, using Urea and Semicarbazide as structure directing agents, was done using following techniques:

1. X-Ray Powder Diffraction (XRD)
2. Infrared Radiation (IR)
3. Scanning electron microscopy (SEM)
4. Elemental Analysis ( C,H,N,S)
5. UV-Vis Diffuse Reflectance Spectroscopy (UV-DRS)

The catalysts are further used for micro-plastic (LDPE) degradation. This is studied with the help of Photocatalytic reactor .It's design and operations are further discussed in this section below.

#### **❖ X-Ray Powder Diffraction (XRD)**

XRD is a non destructive technique used for determining crystal structure of the synthesized compounds. XRD involves constructive interference of monochromatic beam of X-rays and the crystalline samples. It provides information on structures, phases, preferred crystal orientations , average crystallite size, crystal defects etc. When the X-RAY beam falls on the sample at a particular angle and gets diffracted. The constructive interference of the diffracted

x-rays are produced upon satisfying the Bragg's law ( $n\lambda=2d\sin\Theta$ ).The diffracted X-rays are then detected, processed and counted by scanning the sample through a range of  $2\Theta$  angles.

#### ❖ **Infrared Radiation (IR)**

This technique exploits the fact that molecules have specific frequencies at which they rotate or vibrate corresponding to discrete energy levels .In fourier transform infrared technique a beam of infrared light passes through a sample under analysis. When the radiation is equal to the molecular vibration, absorption of radiation takes place. The transmitted light helps us determine the energy absorbed from the incident light.

#### ❖ **Scanning electron microscopy (SEM)**

SEM is a technique used to analyze surface morphology of the synthesized compound. An electron optical system is used to form the electron probe which may be scanned across the surface of the sample in raster pattern. Various signals are generated by interaction of the beam with the sample. These samples are collected and analysed with the application of appropriate detectors.

#### ❖ **UV-Vis Diffuse Reflectance Spectroscopy (UV-DRS)**

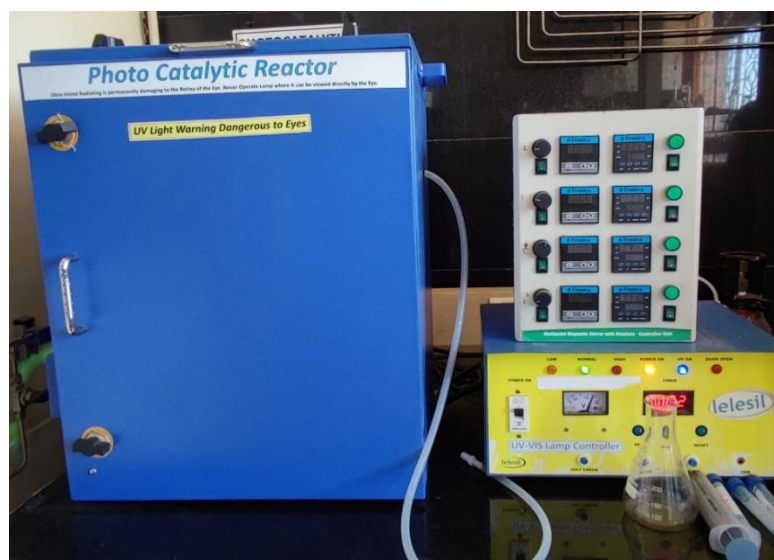
UV-DRS aids in study of opaque solid samples. It works on the principle that not only does light reflected from the material come from the surface but some is reflected internally. When the compound is irradiated the electrons travel from valence band to conduction band. The intensity of the diffused light from the surface of the material is measured as a function of wavelength and it was processed subsequently.

### ❖ **Elemental analysis(C,H,N,S)**

The basic operating principle of CHNS analyser is based on burning of the sample at high temperature. The sample is combusted in a pure oxygen environment. Where carbon, nitrogen, hydrogen and sulphur undergo complete reaction forming  $\text{NO}_2$ ,  $\text{CO}_2$ ,  $\text{SO}_2$ ,  $\text{H}_2\text{O}$  which is detected with the help of thermal conductivity detector.

### ❖ **Photo-catalytic reactor and it's working**

The photo-catalytic reactor used to study micro-plastic degradation consists of a 300 mL quartz vessel equipped with a gas and liquid sampling port. 2 additional ports 1 for temperature while other is for catalyst loading. The source here is a 250 Watt UV lamp. The temperature is maintained through the circulation of cold water through double jacketed chamber. The entire assembly is placed on a Teflon coated magnetic stirrer operating at 1500 RPM. The period, reactor is on is controlled by a programmed digital UV lamp controller unit.



### 3.2 Characterization of MnCo<sub>2</sub>O<sub>4</sub> catalyst

Based on the TGA results, the optimal temperature for obtaining oxides is 500°C for pristine compound (MnCo-1). Manganese cobaltites synthesized using SDA's such as urea (MnCo-2) and semicarbazide (MnCo-3) was calcined at a higher temperature to remove impurities present. As a result, the thermal decomposition of the corresponding precursors was carried out at 500°C and 550°C in furnace for 3 hrs. The X-ray Powder diffraction (XRD) was carried out on a Smartlab Rigaku instrument using Cu K $\alpha$  radiation ( $\lambda = 0.15418$  nm). The XRD peaks of the samples calcined at 500 °C/ 650°C compared with the XRD pattern of Co<sub>3</sub>O<sub>4</sub> confirmed the formation of cobaltites.

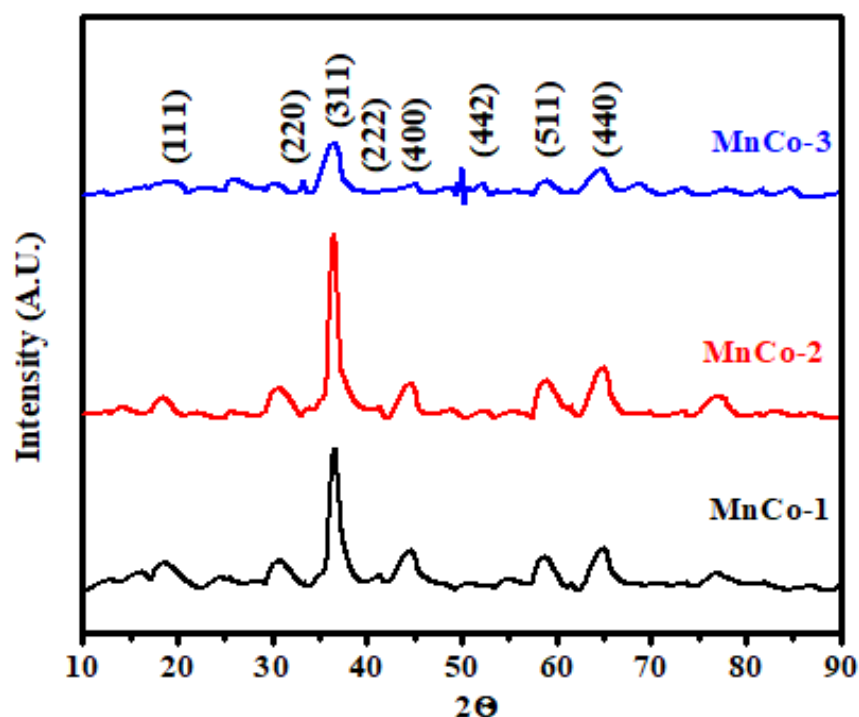


Figure 3: XRD patterns of MnCo<sub>2</sub>O<sub>4</sub> nano-particles (MnCo-1 : Pristine, MnCo-2: Urea , MnCo-3 : Semicarbazide)

Fig 3 gives a closer look at the calcined products formed. The XRD peaks formed can be indexed to the  $\text{MnCo}_2\text{O}_4$  phase with cubic structure (JCPDS No. 23-1237) with  $\text{MnCo}_2\text{O}_4$  lattice constants  $a = 8.269 \text{ \AA}$  considered as mixed-valent oxides that acquire spinel structures in which the Mn and Co ions are distributed over tetrahedral (A) and octahedral (B) sites.

The crystallite sizes of  $\text{MnCo}_2\text{O}_4$  were calculated using the Scherrer equation as follows:

$$D = K\lambda / \beta \cos\Theta$$

Where D is the crystalline size,  $\lambda$  is the X-ray wavelength ( $1.5418 \text{ \AA}$ ),  $\beta$  is the full width at half maximum (FWHM) of the diffraction peak, and  $\theta$  is the Bragg diffraction. The calculations were done considering (311) planes because they had the highest intensity peak for all  $\text{MnCo}_2\text{O}_4$  samples. The crystallite size of  $\text{MnCo}_2\text{O}_4$  was found to range from 4.9 to 8.6 nm, as can be seen from Table 1.4. It is observed that  $\text{MnCo}_2\text{O}_4$  samples give highest crystallite size in pristine conditions followed by the use of urea SDA, The lowest crystallite size of sample was shown in the compound formed using semicarbazide SDA.

Table 1.4: crystallite sizes of the synthesized  $\text{MnCo}_2\text{O}_4$  compounds

| SR.NO. | CODE                    | SDA           | CRYSTALLITE SIZES (nm) |
|--------|-------------------------|---------------|------------------------|
| 1      | $\text{Co}_3\text{O}_4$ | -             | 8.27                   |
| 2      | MnCo-1                  | -             | 7.233                  |
| 3      | MnCo-2                  | UREA          | 8.693                  |
| 4      | MnCo-3                  | SEMICARBAZIDE | 4.989                  |

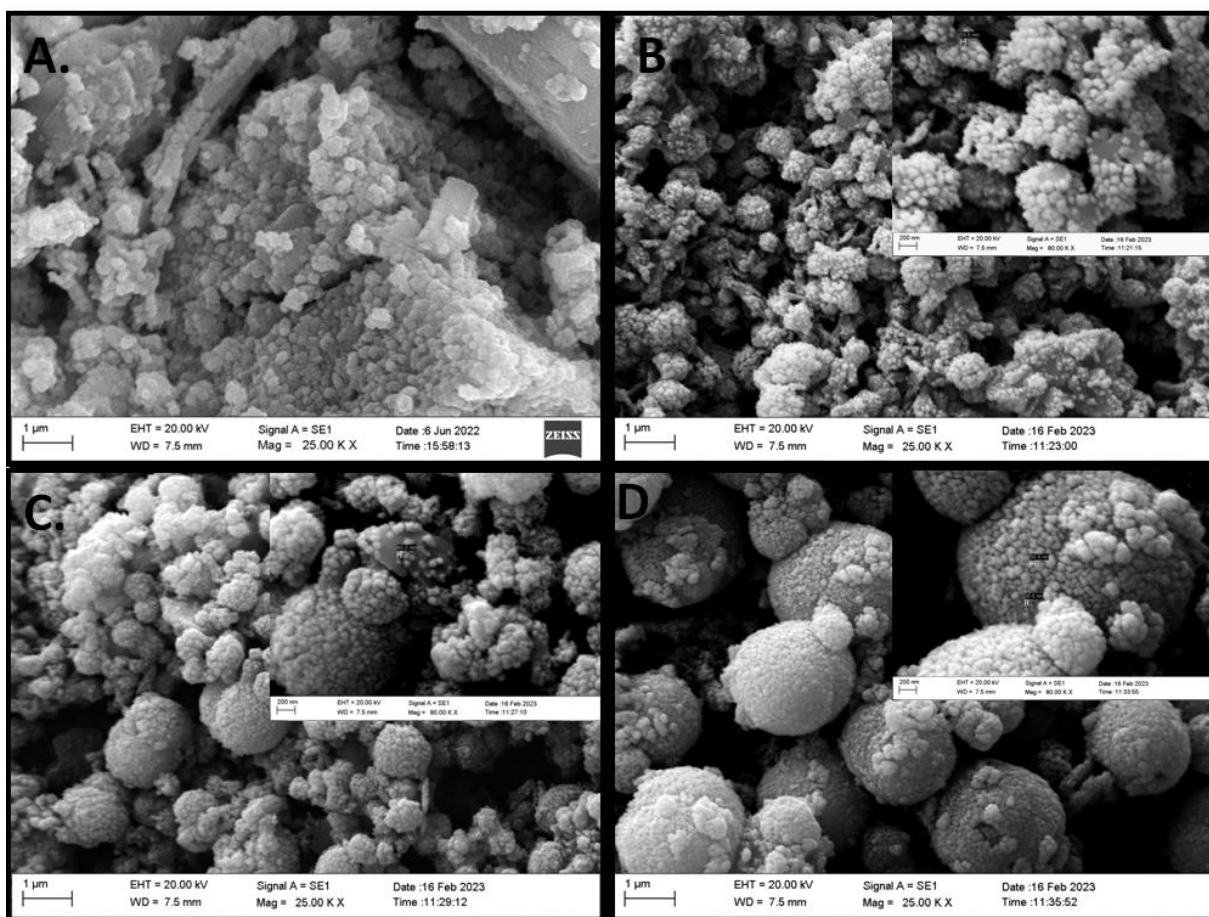


Figure 3.2: SEM images of  $\text{MnCo}_2\text{O}_4$  nano-particles, A:  $\text{Co}_3\text{O}_4$  nano-particles  
 B: Pristine (MnCo-1), C: Urea (MnCo-2), D: Semicarbazide (MnCo-3).

The morphologies and structures of the  $\text{MnCo}_2\text{O}_4$  nano-particles were explored using SEM, Zeiss EV018 as shown in Fig. 3.2. The crystallite sizes acquired from the XRD pattern are much smaller than the particle sizes obtained from the SEM results. SEM shows that  $\text{Co}_3\text{O}_4$  and  $\text{MnCo}_2\text{O}_4$  nanocomposite under pristine conditions show structureless agglomeration (Fig 3.2 B). Under the influence of urea SDA we see incomplete formation of microspheres (Fig 3.2 C). We see formation of complete microspheres when semicarbazide SDA was used (Fig.3.2 D). The SEM images reveal that the size of  $\text{MnCo}_2\text{O}_4$  nano-particles also tend to change with the SDA's used. According to SEM, particle sizes in case of MnCo-1, MnCo-2, MnCo-3 are 58.6 nm, 40.3 nm, 36.6 nm respectively. MnCo-3 showed better morphology than MnCo-1, MnCo-2.

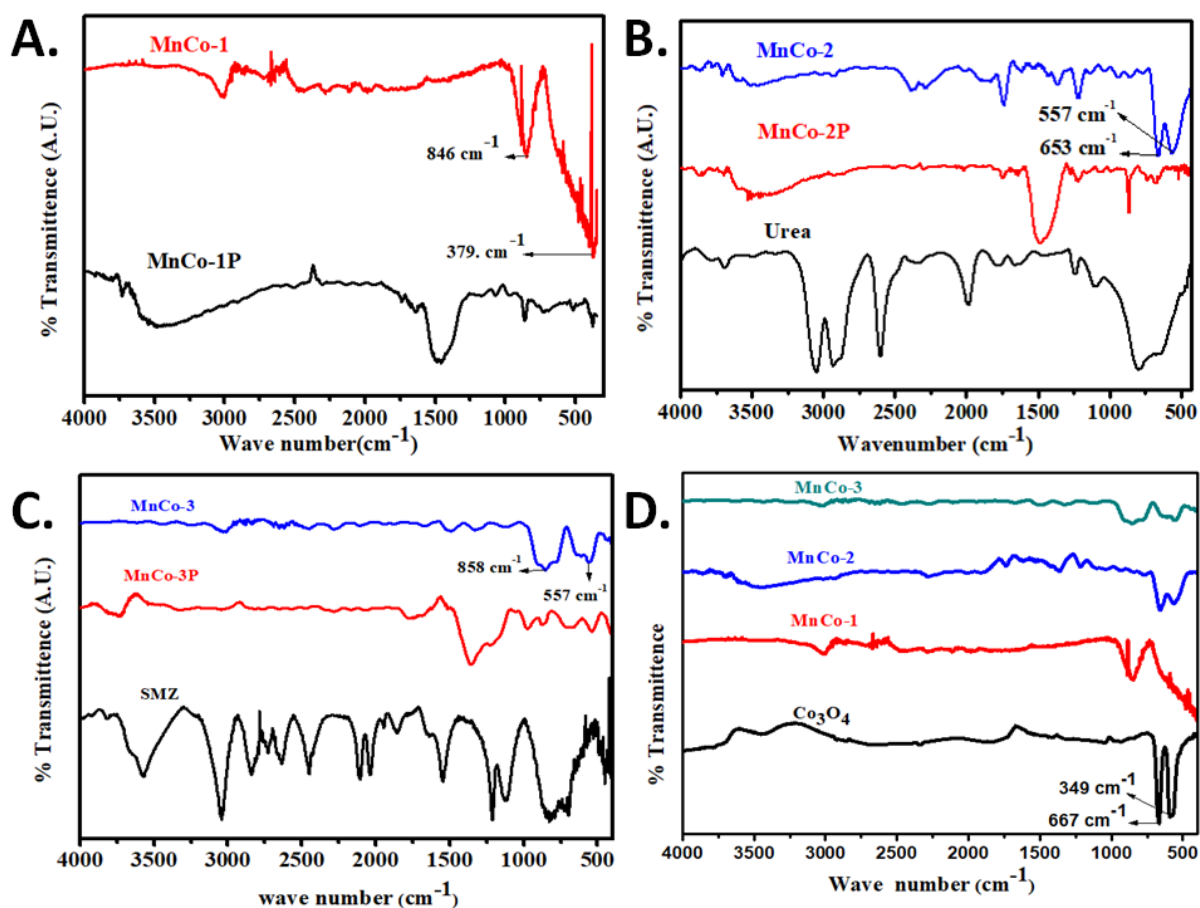


Figure 3.3: FTIR spectra of  $\text{MnCo}_2\text{O}_4$  nanocomposites prepared by co-precipitation method in A) pristine conditions, B) with Urea SDA, C) with Semicarbazide SDA, D) Overlay of  $\text{MnCo}_2\text{O}_4$  nanocomposites prepared by co-precipitation method using various SDA's.

FTIR was done using Shimadzu IR Prestige-21 instrument. FTIR absorption spectra of As synthesized compounds and  $\text{MnCo}_2\text{O}_4$  nano-composites after calcination at  $500^\circ\text{C}$  is shown in fig. 21A .Similar IR spectras for As synthesized and calcined ( $550^\circ\text{C}$  )  $\text{MnCo}_2\text{O}_4$  nano-composites in the presence of SDA's, Urea and semicarbazide are shown in fig.21B and fig. 21C respectively. From fig A-C, we can see that, as synthesized compounds (MnCo-1P, MnCo-2P, MnCo-3P) on calcination at appropriate temperature gives desired metal oxides (MnCo-1, MnCo-2, MnCo-3). Comparing the standard SDA's (urea, semicarbazide ) spectra with MnCo-2, MnCo-3 respectively we can deduce that most of the impurity peaks are not visible in the calcined oxides. In fig. A absorption bands were observed at  $665\text{ cm}^{-1}$  and  $557$

$\text{cm}^{-1}$ . In fig B and C, MnCo-2 and MnCo-3 show similar characteristic peaks at  $653 \text{ cm}^{-1}$ ,  $557 \text{ cm}^{-1}$  and  $663 \text{ cm}^{-1}$ ,  $565 \text{ cm}^{-1}$  respectively.

These peaks are related to the stretching vibrations of Mn–O and Co–O, respectively. The stretching vibrations seen in the FTIR spectras are characteristic of metal oxides in spinel. Fig. D shows broad peaks at around  $3500 \text{ cm}^{-1}$  in MnCo-1, MnCo-2, MnCo-3 spectras due to O-H stretching of absorbed water on nano-particles surface along with the characteristic metal oxide peaks.

Table 1.5 : CHNS data of synthesized  $\text{MnCo}_2\text{O}_4$  compounds.

| SR.NO. | NAME   | N (%) | C (%) | H (%) | S (%) |
|--------|--------|-------|-------|-------|-------|
| 1      | Blank  | 0.26  | 0.05  | 0.143 | 0.02  |
| 2      | MnCo-1 | 0.17  | 0.18  | 0.106 | 0.04  |
| 3      | MnCo-2 | 0.16  | 0.22  | 0.084 | 0.032 |
| 4      | MnCo-3 | 0.20  | 0.16  | 0.096 | 0.035 |

The  $\text{MnCo}_2\text{O}_4$  compounds prepared in pristine conditions and also using SDAs, urea and semicarbazide respectively. They were subjected to Elemental analysis (C, H, N, S) using calibrated Elemental Vario Micro Cube CHNS analyser. The results of the same are shown in table 1.5.

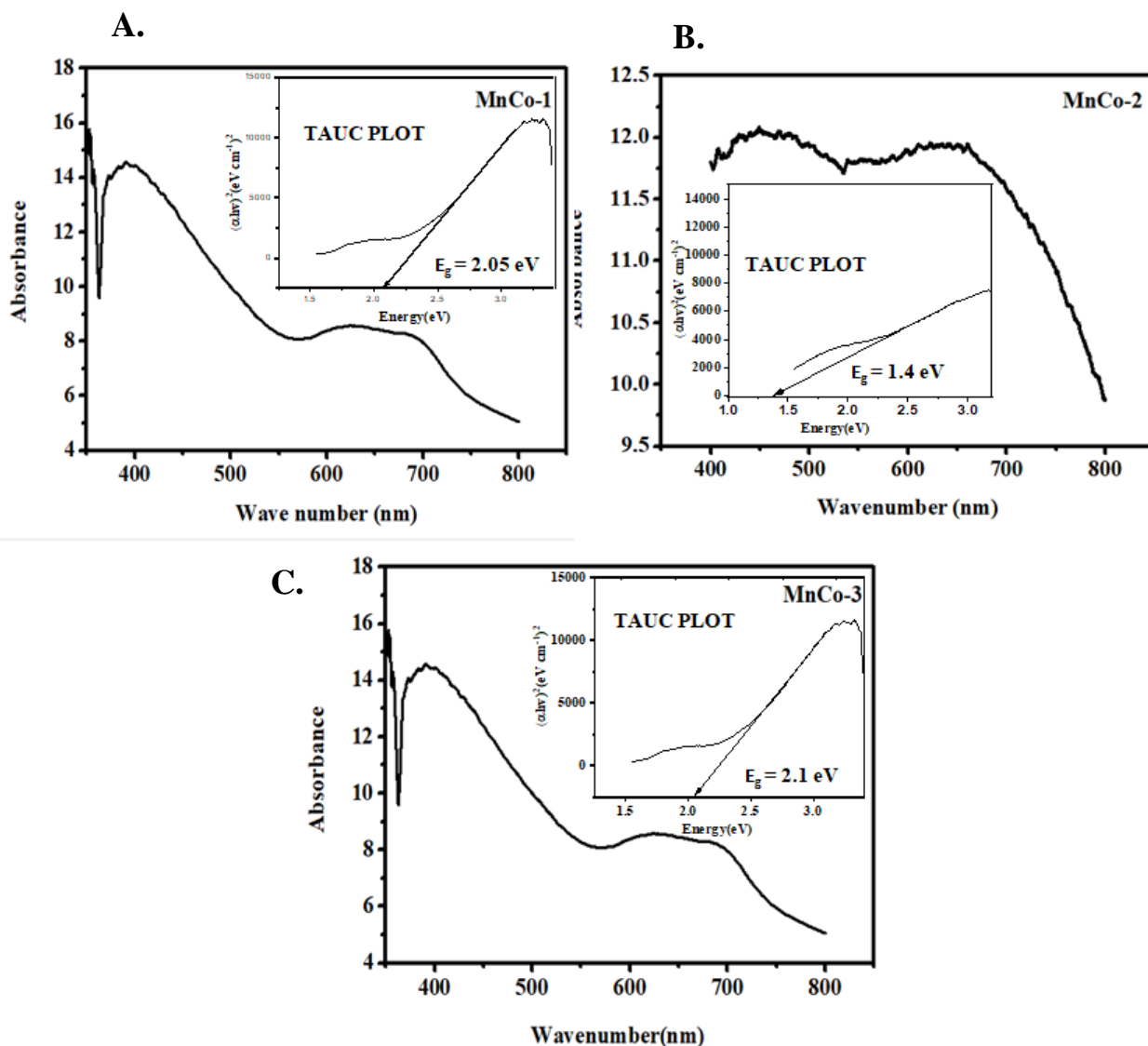


Figure 3.4: shows UV DRS Absorbance plot of A) MnCo-1, B) MnCo-2, C) MnCo-3

UV DRS analysis was done and plotted as seen in Fig. 3.4; two broad peaks are visible in the plots. According to the literature these are the characteristic peaks of mixed metal oxides. The UV-Vis DRS measurement is adopted to estimate the optical properties of samples. All samples display strong light absorption over the entire spectral range (400–800 nm). The addition of secondary ion alters the band gap in the order MnCo-3(2.1 eV) > MnCo-1(2.05 eV) > MnCo-2(1.4 eV)

The characterization of MnCo<sub>2</sub>O<sub>4</sub> nano-particles prepared by coprecipitation method was done using SEM, XRD, IR, UV-DRS and Elemental analysis (C, H, N, S) techniques. The

formation of mixed metal oxide was confirmed through X-Ray diffraction and IR. SEM assisted in deducing the morphology of the synthesized nano-particles, along with the particle size which decreases with the addition of SDA's. UV-DRS were carried out to determine the band gap of nano-particles.

### 3.3 Characterization of $\text{CuCo}_2\text{O}_4$

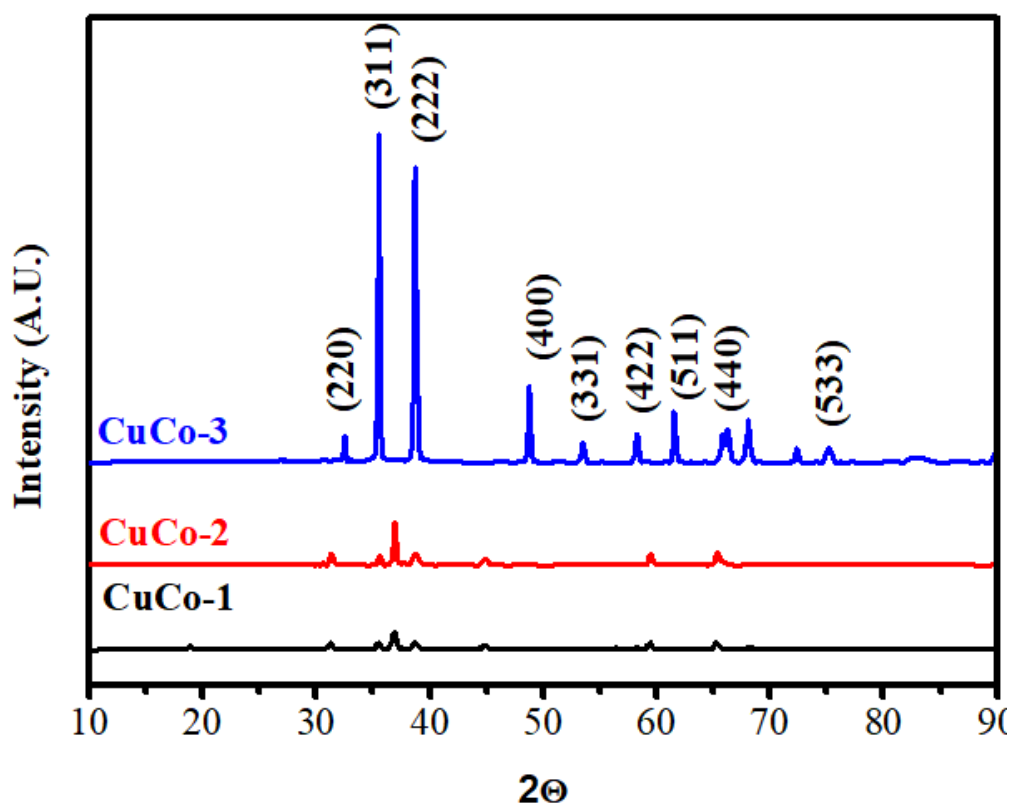


Figure 3.5: XRD patterns of  $\text{CuCo}_2\text{O}_4$  nano-particles (CuCo-1: Pristine, CuCo-2: Urea, CuCo-3 : Semicarbazide)

Figure 3.5 showcases an XRD of  $\text{CuCo}_2\text{O}_4$  samples under pristine conditions and also under the use of SDA's urea and semicarbazide. Rigaku instrument using  $\text{Cu K}\alpha$  radiation ( $\lambda = 0.15418 \text{ nm}$ ) used for sample analysis showed well defined diffraction peaks point to a cubic spinel  $\text{CuCo}_2\text{O}_4$  (JCPDS NO. 80-1532) structure. Table 1.6 showcases the crystallite sizes of the samples. The sharp peaks for the sample CuCo-3 confirm its high crystallinity

Table 1.6: crystallite size of the synthesized  $\text{CuCo}_2\text{O}_4$  compounds

| SR.NO. | CODE                    | SDA           | CRYSTALLITE SIZES (nm) |
|--------|-------------------------|---------------|------------------------|
| 1      | $\text{Co}_3\text{O}_4$ | -             | 8.27                   |
| 2      | CuCo-1                  | -             | 18.9                   |
| 3      | CuCo-2                  | UREA          | 32.57                  |
| 4      | CuCo-3                  | SEMICARBAZIDE | 37.44                  |

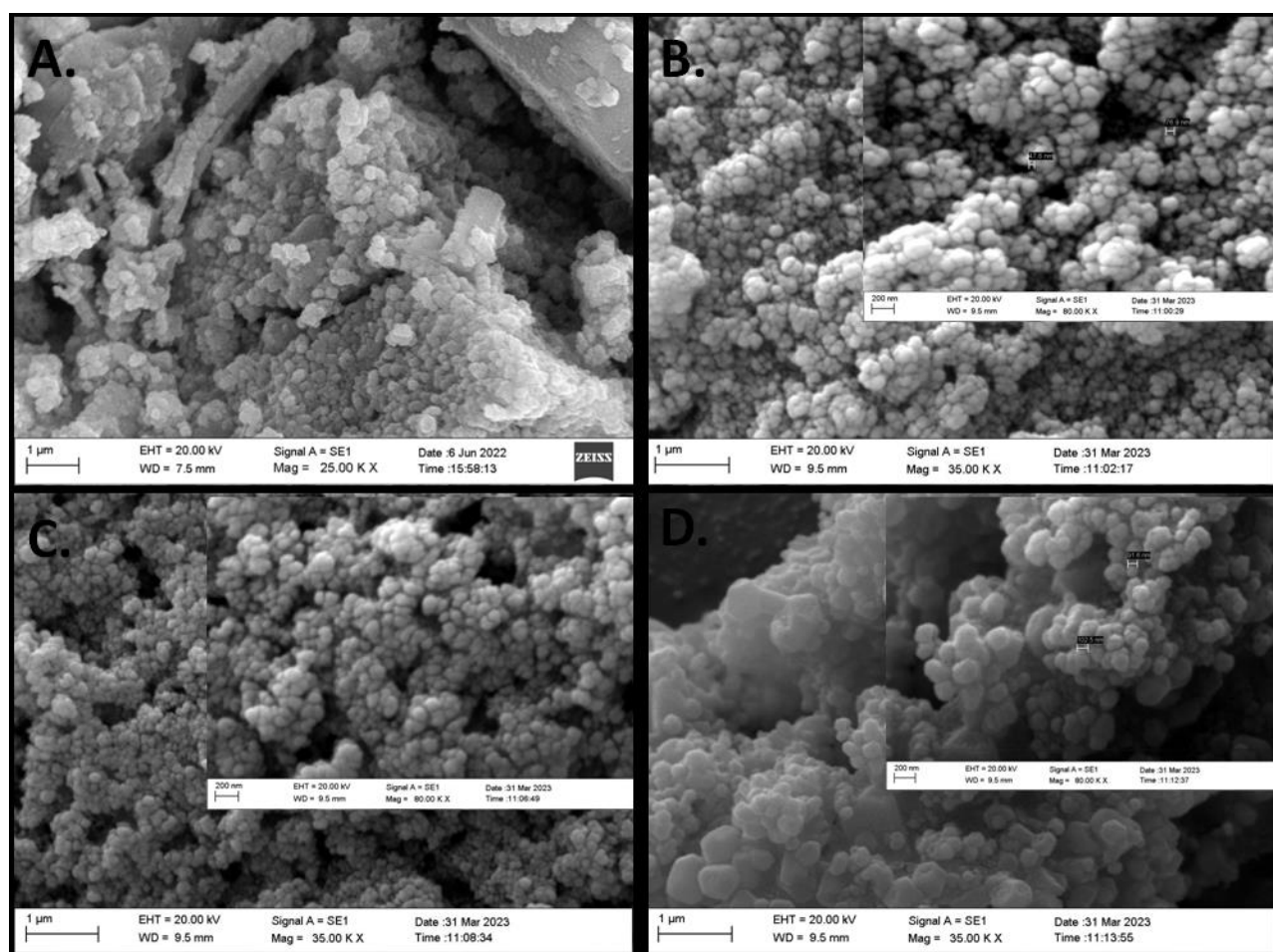


Figure 3.6: SEM images of  $\text{CuCo}_2\text{O}_4$  nano-particles with SDAs , A:  $\text{Co}_3\text{O}_4$  nano-particles B: Pristine (MnCo-1), C: Urea (MnCo-2), D: Semicarbazide (MnCo-3).

The morphologies of copper cobaltites samples under pristine conditions and on using SDA's were agglomerated. They showed cauliflower like structures. From SEM tentative sizes shown by CuCo-1, CuCo-2 and CuCo-3 were 47.6 nm, 73.2 nm and 91.6 nm respectively. This increase in sizes from pristine to urea to semicarbazide is in alignment with the XRD data but differs from manganese cobaltite samples which showed opposite trend.

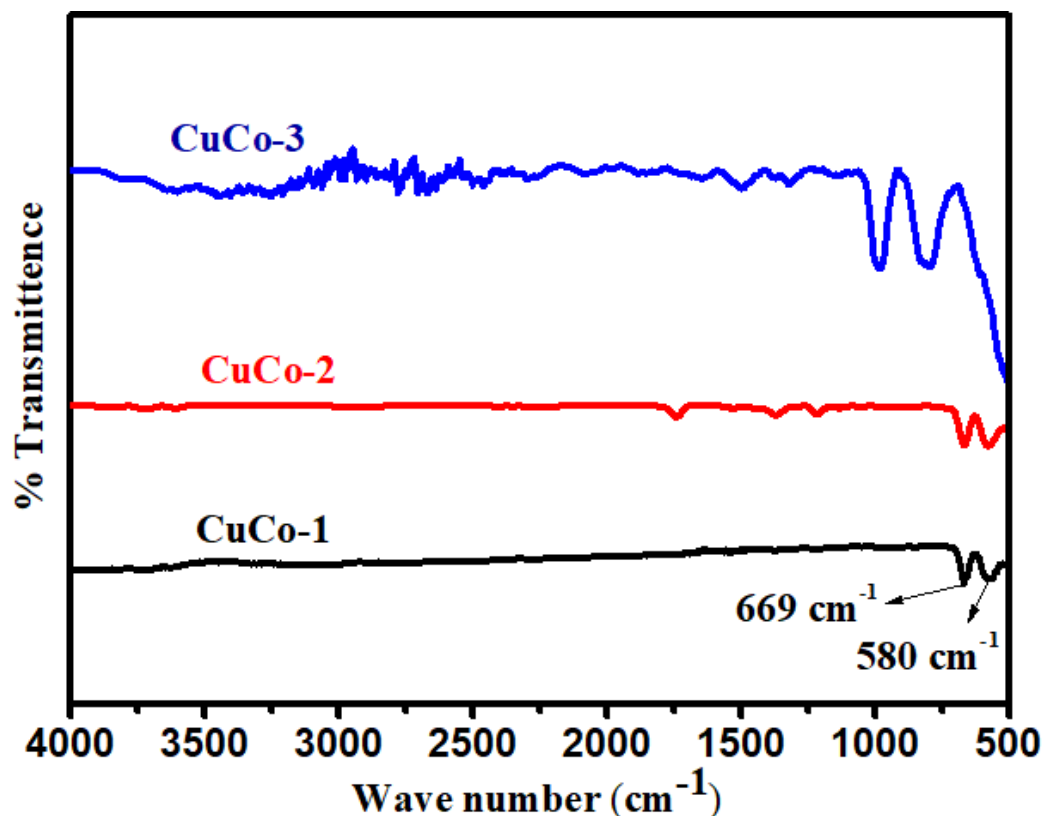


Figure 3.3: FTIR spectra of CuCo<sub>2</sub>O<sub>4</sub> nanocomposites prepared by co-precipitation method using urea and semicarbazide SDA's.

The FT-IR spectrum of CuCo<sub>2</sub>O<sub>4</sub> shows two major sharp peaks in the range of 500–700 cm<sup>-1</sup> which are due to the metal–oxygen vibrational modes at the tetrahedral- and octahedral-sites, respectively. The peaks seen between 3000–3500 cm<sup>-1</sup> and 1600 cm<sup>-1</sup> can be attributed to the stretching and bending vibrations of free or absorbed water molecules<sup>41</sup>.

Table 1.7: CHNS data of synthesized  $\text{CuCo}_2\text{O}_4$  compounds.

| SR.NO. | NAME   | N (%) | C (%) | H (%) | S (%) |
|--------|--------|-------|-------|-------|-------|
| 1      | Blank  | 0.00  | 0.00  | 0.00  | 0.00  |
| 2      | CuCo-1 | 0.44  | 0.29  | 0.317 | 0.061 |
| 3      | CuCo-2 | 0.41  | 0.10  | 0.631 | 0.025 |
| 4      | CuCo-3 | 0.41  | 0.08  | 0.049 | 0.011 |

The  $\text{CuCo}_2\text{O}_4$  compounds were prepared in pristine conditions and also using SDAs, urea and semicarbazide respectively. They were subjected to Elemental analysis (C, H, N, S) using calibrated Elemental Vario Micro Cube CHNS analyser. The results of the same are shown in table1.7.

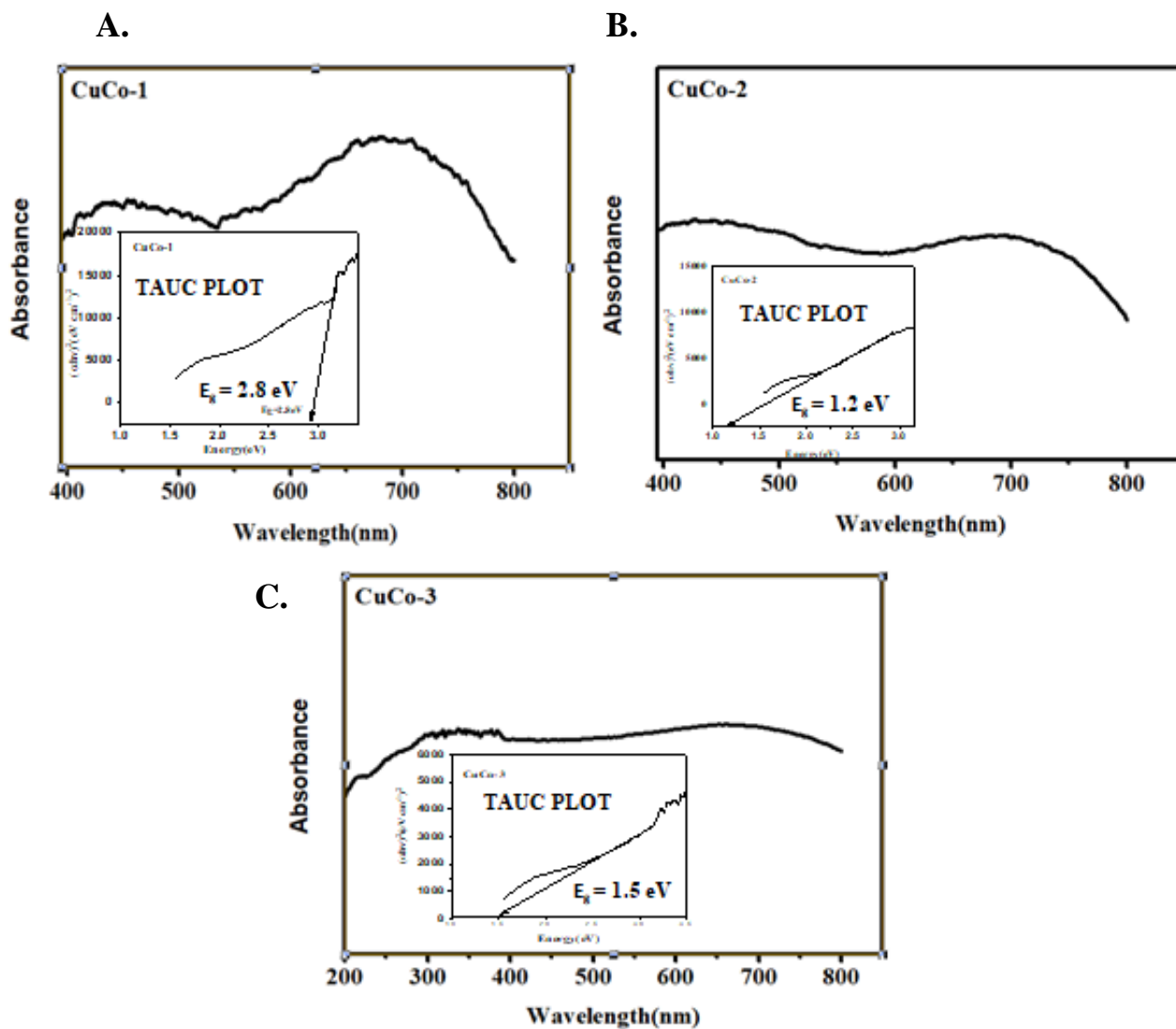


Figure 3.7: shows UV DRS Absorbance plot of A) CuCo-1, B) CuCo-2, C) CuCo-3

From figure 3.7 we can determine that copper cobaltite in pristine condition shows the highest band gap of 2.8 eV followed by CuCo-3 with band gap 1.5 eV. CuCo-2 shows the lowest band gap of 1.2 eV. Hence it is expected for CuCo-1 to show higher Photo-catalytic activity than other copper cobaltite catalysts.

# CHAPTER IV

#### **4.0 Photo-catalytic activity**

The synthesized Manganese and Copper cobaltites were screened for photo-catalytic activity.  $MnCo_2O_4$  and  $CuCo_2O_4$  synthesized under pristine conditions (MnCo-1, CuCo-1) and along with SDA's urea (MnCo-2, CuCo-2) and semicarbazide (MnCo-3, CuCo-3) respectively were used to photo-catalytically degrade Methylene Blue (MB) and LDPE micro-plastic .

#### **4.1 Photo-catalytic degradation of methylene blue**

A 30 ppm methylene blue solution was prepared in a 1000 mL conical flask. 100 mg of the catalyst was added to the 300 mL of above mentioned solution. It was further sonicated for 5 minutes. The solution was then added in the flask and placed in the photocatalytic reactor under 250 W UV light lamp for 1 hour. Aliquots were removed every 10 minutes, which were filtered and centrifuged for 20 minutes. Absorbance of the aliquots was recorded using a colorimeter, at  $\lambda_{max}$  620 nm.

It was observed that catalysts MnCo-1, MnCo-2, CuCo-1, CuCo-2, and CuCo-3 showed constant absorbance even after the solution was exposed to UV light for 60 minutes. Whereas in case of MnCo-3 (semicarbazide as SDA) slight degradation was seen as seen from table 1.8 and figure 4.0 respectively

Table 1.8: Absorbance values of Methylene blue with time using catalyst MnCo-3

| TIME (Min) | ABSORBANCE | CONCENTRATION (ppm) |
|------------|------------|---------------------|
| 0          | 0.76       | 30                  |
| 10         | 0.74       | 29.21               |
| 20         | 0.71       | 28.02               |
| 30         | 0.69       | 27.23               |
| 40         | 0.66       | 26.05               |
| 50         | 0.62       | 24.47               |
| 60         | 0.62       | 24.47               |

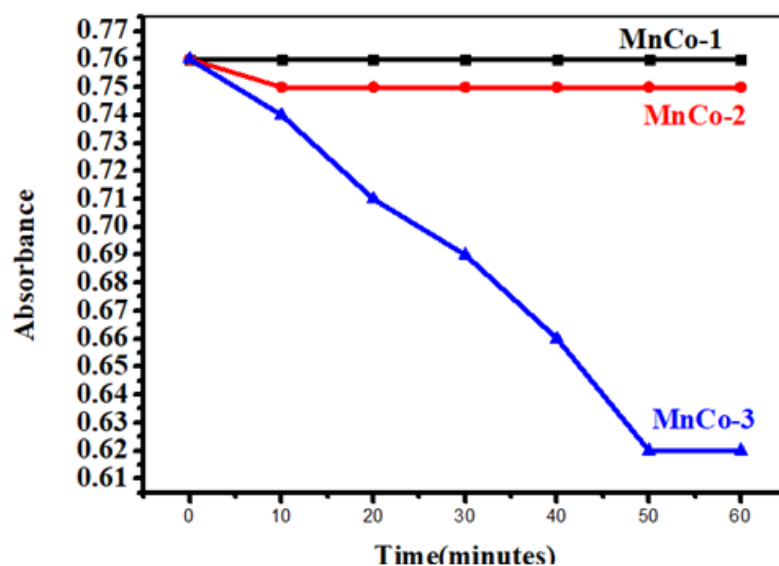


Figure 4.0 Absorbance VS time plot of MB with manganese cobaltites ,without and with urea and semicarbazide SDAs

The Percentage degradation was determined using below mentioned formula. It is determined that the % degradation of MB on using MnCo-3 catalyst is 18.43%.

$$\% = (C_0 - C_1 / C_0) * 100$$

Where  $C_1$  is final Concentration,  $C_0$  is initial concentration and % is percent degradation

#### **4.2 Photo-catalytic degradation of LDPE micro-plastics**

MnCo-1, MnCo-2, MnCo-3, CuCo-1, CuCo-2, CuCo-3 were used to catalyse degradation of micro-plastics. It was observed that while other catalysts showed no degradation, CuCo-3 catalysed LDPE showcased slight degradation. This can be confirmed from Sem images (Figure 4.1) and IR spectra (Figure 4.2).

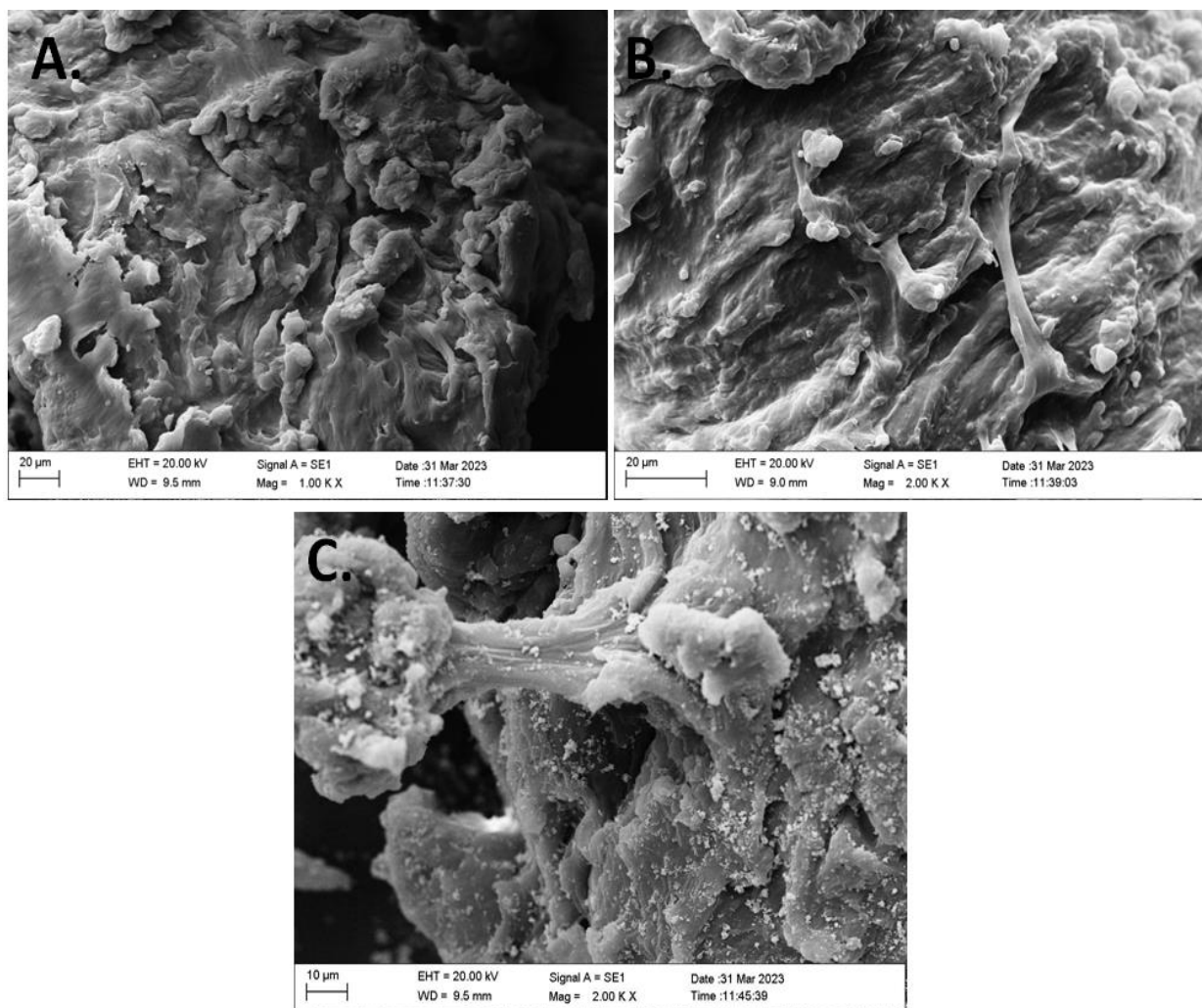


Figure 4.1: SEM images of LDPE micro-plastics A: Before irradiation, B: After 5 hr irradiation catalysed by MnCo-3, C-D: After 5 hr irradiation catalysed by CuCo-3

Figure 4.1A, Sem image of non irradiated LDPE shows a smooth surface with few cracks and crevices due to few manufacturing defects and spots<sup>24</sup>. Sem image (Figure 4.1B) of LDPE degraded using MnCo-3 catalyst showed few stretch marks but still a continuous surface. CuCo-3 catalysed LDPE degradation (Figure 4.1 C-D) resulted in much more discontinuous surface with cracks and crevices. Figure 4.1 D showcases the cleavage formed on the surface of the micro-plastic.

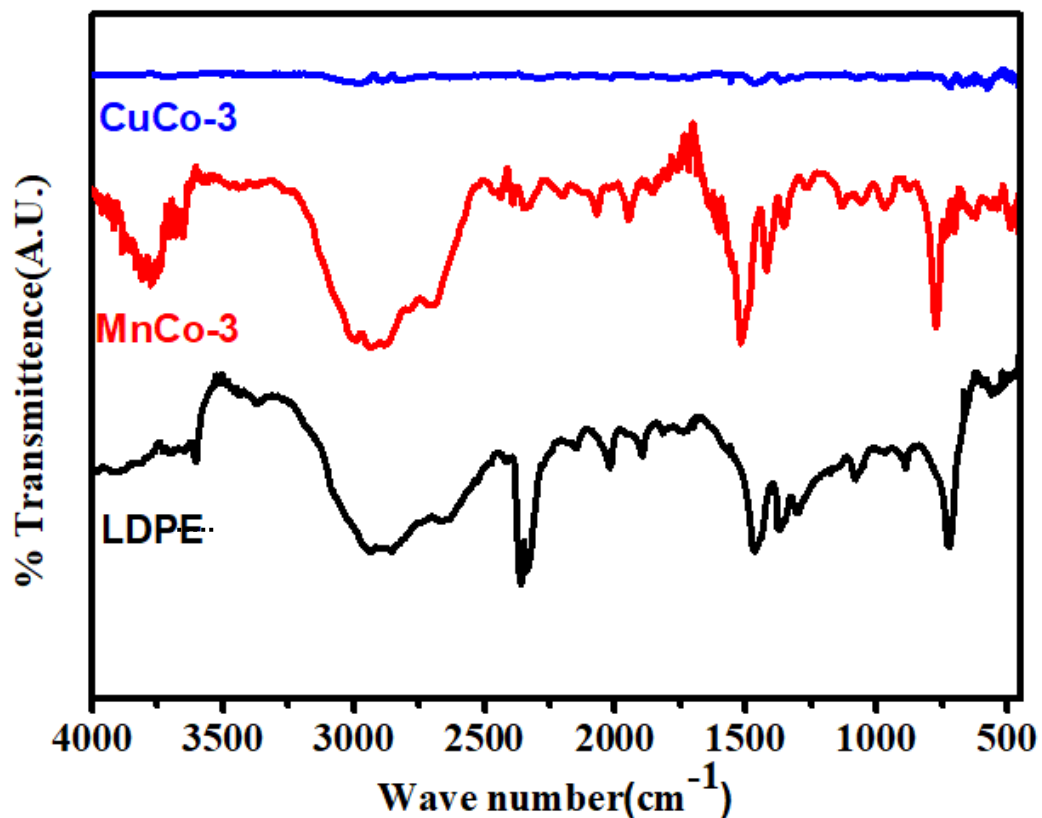


Figure 4.2: FTIR of LDPE micro-plastics A: Before irradiation, B: After 5 hr irradiation catalysed by MnCo-3, C-D:After 5 hr irradiation catalysed by CuCo-3

Figure 4.2 displays FTIR of an irradiated LDPE, LDPE after 5 hr UV-irradiation catalysed by MnCo-3 and LDPE after 5 hr UV-irradiation catalysed by CuCo-3. It is observed that most of the peaks seen in an irradiated LDPE and MnCo-3 catalysed degraded LDPE are similar. Inferring that no degradation has occurred. While CuCo-3 catalysed degraded LDPE do not show any such peaks concluding that degradation of LDPE has occurred.

## CONCLUSION

In this study we have carried out photo-catalytic degradation of toxic dyes and microplastic using  $\text{MnCo}_2\text{O}_4$  and  $\text{CuCo}_2\text{O}_4$  synthesized by co-precipitation in the presence of urea and semicarbazide SDAs. The degradation was carried out using a 250 Watts UV lamp in a photo-reactor.

It was observed that  $\text{MnCo}_2\text{O}_4$  synthesized using semicarbazide (MnCo-3) showed better morphology and lower crystallite size followed by  $\text{MnCo}_2\text{O}_4$  assisted by urea SDA (MnCo-2) and then  $\text{MnCo}_2\text{O}_4$  with no SDA (MnCo-1). Apart from MnCo-2, MnCo-1 and MnCo-3 showed crystallite sizes lower than  $\text{Co}_3\text{O}_4$ . A contrary trend was seen in case of  $\text{CuCo}_2\text{O}_4$ . The crystallite sizes were much higher than that of  $\text{Co}_3\text{O}_4$ . Copper cobaltite prepared with semicarbazide SDA (CuCo-3), followed by  $\text{CuCo}_2\text{O}_4$  with urea SDA (CuCo-2) and the least crystallite size was given in pristine conditions (CuCo-1). This trend is attributed to the higher atomic size of copper than manganese.

In photo-catalytic degradation of Methylene Blue, it was found that MnCo-3 showed 18.43% degradation; while other catalysts didn't exhibit any significant degradation. This can be attributed to its high band gap of 2.8 eV. CuCo-3 showed photo-catalytic degradation in LDPE micro-plastics. While other micro-plastics didn't show any changes on the plastic surface, in case of CuCo-3 cracks were present and cleavage formation was witnessed. The degradation procedure needs further optimization to increase the efficiency of the photo-catalytic degradation.

## **BIBLIOGRAPHY**

- (1) Hao, D.; Xie, Y.; Wang, J. Microplastic Degradation Methods and Corresponding Degradation Mechanism : Research Status and Future Perspectives. *J. Hazard. Mater.* **2021**, *418* (June), 126377. <https://doi.org/10.1016/j.jhazmat.2021.126377>.
- (2) Lastovina, T. A.; Budnyk, A. P. A Review of Methods for Extraction, Removal, and Stimulated Degradation of Microplastics. *J. Water Process Eng.* **2021**, *43* (May), 102209. <https://doi.org/10.1016/j.jwpe.2021.102209>.
- (3) Bratovcic, A. Degradation of Micro-and Nano-Plastics by Photocatalytic Methods Cite This Paper Related Papers Degradation of Micro-and Nano-Plastics by Photocatalytic Methods. *J. Nanosci. Nanotechnol. Appl.* **2011**.
- (4) Zhang, K.; Hamidian, A. H.; Tubić, A.; Zhang, Y.; Fang, J. K. H.; Wu, C.; Lam, P. K. S. Understanding Plastic Degradation and Microplastic Formation in the Environment: A Review. *Environ. Pollut.* **2021**, *274*. <https://doi.org/10.1016/j.envpol.2021.116554>.
- (5) Xu, Q.; Huang, Q. S.; Luo, T. Y.; Wu, R. L.; Wei, W.; Ni, B. J. Coagulation Removal and Photocatalytic Degradation of Microplastics in Urban Waters. *Chem. Eng. J.* **2021**, *416* (February), 129123. <https://doi.org/10.1016/j.cej.2021.129123>.
- (6) Saboor, F. H.; Hadian-Ghazvini, S.; Torkashvand, M. Microplastics in Aquatic Environments: Recent Advances in Separation Techniques. *Period. Polytech. Chem. Eng.* **2022**, *66* (2), 167–181. <https://doi.org/10.3311/PPch.18930>.
- (7) Hale, R. C.; Seeley, M. E.; La Guardia, M. J.; Mai, L.; Zeng, E. Y. A Global Perspective on Microplastics. *J. Geophys. Res. Ocean.* **2020**, *125* (1), 1–40. <https://doi.org/10.1029/2018JC014719>.
- (8) Nabi, I.; Bacha, A. U. R.; Ahmad, F.; Zhang, L. Application of Titanium Dioxide for the Photocatalytic Degradation of Macro- and Micro-Plastics: A Review. *J. Environ. Chem. Eng.* **2021**, *9* (5), 105964. <https://doi.org/10.1016/j.jece.2021.105964>.
- (9) Pham, T. H.; Do, H. T.; Phan Thi, L. A.; Singh, P.; Raizada, P.; Chi-Sheng Wu, J.; Nguyen, V. H. Global Challenges in Microplastics: From Fundamental Understanding to Advanced Degradations toward Sustainable Strategies. *Chemosphere* **2021**, *267*, 129275. <https://doi.org/10.1016/j.chemosphere.2020.129275>.
- (10) Arpia, A. A.; Chen, W.; Ubando, A. T.; Raza, S.; Culaba, A. B. Microplastic Degradation as a Sustainable Concurrent Approach for Producing Biofuel and Obliterating Hazardous Environmental Effects : A State-of-the-Art Review. *J. Hazard. Mater.* **2021**, *418* (June), 126381. <https://doi.org/10.1016/j.jhazmat.2021.126381>.

- (11) Khan, M. M.; Adil, S. F.; Al-Mayouf, A. Metal Oxides as Photocatalysts. *J. Saudi Chem. Soc.* **2015**, *19* (5), 462–464. <https://doi.org/10.1016/j.jscs.2015.04.003>.
- (12) Low, J.; Yu, J.; Jaroniec, M.; Wageh, S.; Al-Ghamdi, A. A. Heterojunction Photocatalysts. *Adv. Mater.* **2017**, *29* (20), 1–20. <https://doi.org/10.1002/adma.201601694>.
- (13) Arora, A. K.; Jaswal, V. S.; Singh, K.; Singh, R. Applications of Metal/Mixed Metal Oxides as Photocatalyst: A Review. *Orient. J. Chem.* **2016**, *32* (4), 2035–2042. <https://doi.org/10.13005/ojc/320430>.
- (14) Wang, J.; Jiang, Y.; Gao, C.; Li, Y.; Wu, X. Synergistic Effect of Bimetal in Three-Dimensional Hierarchical MnCo<sub>2</sub>O<sub>4</sub> for High Efficiency of Photoinduced Fenton-like Reaction. *Surfaces and Interfaces* **2021**, *27* (June), 101482. <https://doi.org/10.1016/j.surfin.2021.101482>.
- (15) Raya, I.; Widjaja, G.; Hachem, K.; Rodin, M. N.; Ali, A. A.; Kadhim, M. M.; Mustafa, Y. F.; Mahmood, Z. H.; Aravindhan, S. MnCo<sub>2</sub>O<sub>4</sub>/Co<sub>3</sub>O<sub>4</sub> Nanocomposites: Microwave-Assisted Synthesis, Characterization and Photocatalytic Performance. *J. Nanostructures* **2021**, *11* (4), 728–735. <https://doi.org/10.22052/JNS.2021.04.010>.
- (16) Kim, J. W.; Lee, S. J.; Biswas, P.; Lee, T. II; Myoung, J. M. Solution-Processed n-ZnO Nanorod/p-Co<sub>3</sub>O<sub>4</sub> Nanoplate Heterojunction Light-Emitting Diode. *Appl. Surf. Sci.* **2017**, *406*, 192–198. <https://doi.org/10.1016/j.apsusc.2017.02.129>.
- (17) Basaleh, A. S.; Mahmoud, M. H. H. MnCo<sub>2</sub>O<sub>4</sub>@ZrO<sub>2</sub> Nanocomposites Prepared via Facile Route toward Photoreduction of Hg (II) Ions. *Opt. Mater. (Amst)*. **2022**, *125* (January), 112135. <https://doi.org/10.1016/j.optmat.2022.112135>.
- (18) Xu, C.; Jin, C.; Chang, W.; Hu, X.; Deng, H.; Liu, E.; Fan, J. Interfacially Bonded CuCo<sub>2</sub>O<sub>4</sub>/TiO<sub>2</sub> Nanosheet Heterostructures for Boosting Photocatalytic H<sub>2</sub> Production. *Catal. Sci. Technol.* **2019**, *9* (18), 4990–5000. <https://doi.org/10.1039/c9cy01209e>.
- (19) Liang, Q.; Liu, X.; Zeng, G.; Liu, Z.; Tang, L.; Shao, B.; Zeng, Z.; Zhang, W.; Liu, Y.; Cheng, M.; Tang, W.; Gong, S. Surfactant-Assisted Synthesis of Photocatalysts: Mechanism, Synthesis, Recent Advances and Environmental Application. *Chem. Eng. J.* **2019**, *372* (February), 429–451. <https://doi.org/10.1016/j.cej.2019.04.168>.
- (20) Sen, S. K.; Raut, S. Journal of Environmental Chemical Engineering Microbial Degradation of Low Density Polyethylene ( LDPE ): A Review. *Biochem. Pharmacol.* **2015**. <https://doi.org/10.1016/j.jece.2015.01.003>.
- (21) Tofa, T. S.; Laxman, K.; Swaraj, K.; Joydeep, P. Visible Light Photocatalytic

- Degradation of Microplastic Residues with Zinc Oxide Nanorods. *Environ. Chem. Lett.* **2019**, No. 0123456789. <https://doi.org/10.1007/s10311-019-00859-z>.
- (22) Khan, Z.; Voice, T. C.; Tahir, C. Photocatalytic Degradation of Low Density Polyethylene ( LDPE ) Films Using Titania Nanotubes. *Environ. Nanotechnology, Monit. &#x0026; Manag.* **2016**. <https://doi.org/10.1016/j.enmm.2016.01.001>.
- (23) Estefan, B.; Manuel, J. First Insights into Photocatalytic Degradation of HDPE and LDPE Microplastics by a Mesoporous N – TiO<sub>2</sub> Coating : E Ff Ect of Size and Shape of Microplastics. *Coatings* **2020**.
- (24) Zinc, P.; Nanorod, O.; Tofa, T. S.; Ye, F.; Kunjali, K. L. Enhanced Visible Light Photodegradation of Microplastic Fragments with Plasmonic. *Catalysts* **2019**.
- (25) Kamalian, P.; Khorasani, S. N.; Abdolmaleki, A.; Karevan, M.; Khalili, S.; Shirani, M.; Neisiany, R. E. Toward the Development of Polyethylene Photocatalytic Degradation. *DE GRUYTER* **2020**, 40 (2), 181–191.
- (26) Venkataramana, C.; Botsa, S. M.; Shyamala, P.; Muralikrishna, R. Photocatalytic Degradation of Polyethylene Plastics by NiAl<sub>2</sub>O<sub>4</sub> Spinel-Synthesis and Characterization. *ECSN* **2020**, 129021. <https://doi.org/10.1016/j.chemosphere.2020.129021>.
- (27) Alabi, O. A.; Ologbonjaye, K. Toxicology and Risk Assessment Public and Environmental Health Effects of Plastic Wastes Disposal : *J. Toxicol. risk Assess.* **2019**, No. August. <https://doi.org/10.23937/2572-4061.1510021>.
- (28) Nabi, I.; Bacha, A.; Li, K.; Cheng, H.; Wang, T.; Liu, Y.; Ajmal, S.; Yang, Y.; Feng, Y.; Zhang, L. Complete Photocatalytic Mineralization of Microplastic on TiO<sub>2</sub> Nanoparticle Film. *ISCIENCE* **2020**, 101326. <https://doi.org/10.1016/j.isci.2020.101326>.
- (29) Kemp, T. J.; McIntyre, R. A. Influence of Transition Metal-Doped Titanium ( IV ) Dioxide on the Photodegradation of Polystyrene. *Polym. Degrad. Stab.* **2006**, 91, 3010–3019. <https://doi.org/10.1016/j.polymdegradstab.2006.08.005>.
- (30) Wang, L.; Kaeppler, A.; Fischer, D.; Simmchen, J. Photocatalytic TiO<sub>2</sub> Micromotors for Removal of Microplastics and Suspended Matter. *Appl. Mater. interfaces* **2019**, 5–12. <https://doi.org/10.1021/acsami.9b06128>.
- (31) Zhou, D.; Wang, L.; Zhang, F.; Wu, J.; Wang, H.; Yang, J. Feasible Degradation of Polyethylene Terephthalate Fiber-Based Microplastics in Alkaline Media with Bi<sub>2</sub>O<sub>3</sub>@N-TiO<sub>2</sub> Z-Scheme Photocatalytic System. *Adv. Sustain. Syst.* **2022**, 6 (5). <https://doi.org/10.1002/adsu.202100516>.

- (32) Martí, A.; Torres-martí, L. M. Photo-Oxidative Degradation of TiO<sub>2</sub> / Polypropylene Films. *Mater. Res. Bull.* **2014**, *51*, 56–62.  
<https://doi.org/10.1016/j.materresbull.2013.11.040>.
- (33) Kamrannejad, M. M.; Hasanzadeh, A.; Nosoudi, N.; Mai, L.; Babaluo, A. A.; Ave, H. Photocatalytic Degradation of Polypropylene/TiO<sub>2</sub> Nano-Composites. *Mater. Res.* **2014**, *17* (4), 1039–1046.
- (34) Razali, N. A.; Rafizah, W. A. N.; Abdullah, W. A. N.; Zikir, M. EFFECT OF THERMO-PHOTOCATALYTIC PROCESS USING ZINC OXIDE ON DEGRADATION OF MACRO / MICRO-PLASTIC IN AQUEOUS ENVIRONMENT. *J. Sustain. Sci. Manag.* **2020**, *15* (6), 1–14.
- (35) Uheida, A.; Mejía, H. G. Visible Light Photocatalytic Degradation of Polypropylene Microplastics in a Continuous Water Flow System. *J. Hazard. Mater.* **2020**, 124299.  
<https://doi.org/10.1016/j.jhazmat.2020.124299>.
- (36) Ariza-Tarazona, M. C.; Villarreal-Chiu, J. F.; Barbieri, V.; Siligardi, C.; Cedillo-González, E. I. New Strategy for Microplastic Degradation: Green Photocatalysis Using a Protein-Based Porous N-TiO<sub>2</sub> Semiconductor. *Ceram. Int.* **2019**, *45* (7), 9618–9624. <https://doi.org/10.1016/j.ceramint.2018.10.208>.
- (37) Fadli, M. H.; Ibadurrohman, M.; Slamet, S. Microplastic Pollutant Degradation in Water Using Modified TiO<sub>2</sub> Microplastic Pollutant Degradation in Water Using Modified TiO<sub>2</sub> Photocatalyst Under UV-Irradiation. **2021**.  
<https://doi.org/10.1088/1757-899X/1011/1/012055>.
- (38) Cao, B.; Wan, S.; Wang, Y.; Guo, H.; Ou, M.; Zhong, Q. Journal of Colloid and Interface Science Highly-Efficient Visible-Light-Driven Photocatalytic H<sub>2</sub> Evolution Integrated with Microplastic Degradation over MXene / Zn<sub>x</sub>Cd<sub>1-x</sub>S Photocatalyst. *J. Colloid Interface Sci.* **2022**, *605*, 311–319.  
<https://doi.org/10.1016/j.jcis.2021.07.113>.
- (39) Jiang, R.; Lu, G.; Yan, Z.; Liu, J.; Wu, D.; Wang, Y. Microplastic Degradation by Hydroxy-Rich Bismuth Oxychloride. *J. Hazard. Mater.* **2020**, 124247.  
<https://doi.org/10.1016/j.jhazmat.2020.124247>.
- (40) Oladoye, P. O.; Ajiboye, T. O.; Omotola, E. O.; Oyewola, O. J. Methylene Blue Dye: Toxicity and Potential Elimination Technology from Wastewater. *Results Eng.* **2022**, *16* (August), 100678. <https://doi.org/10.1016/j.rineng.2022.100678>.
- (41) Nekoeinia, M.; Salehriahi, F.; Moradlou, O.; Kazemi, H.; Yousefinejad, S. Enhanced Fenton-like Catalytic Performance of N-Doped Graphene Quantum Dot Incorporated

CuCo<sub>2</sub>O<sub>4</sub>. *New J. Chem.* **2018**, 42 (11), 9209–9220.

<https://doi.org/10.1039/c8nj00219c>.

- (42) Habibi, M. H.; Bagheri, P. Enhanced Photo-Catalytic Degradation of Naphthol Blue Black on Nano-Structure MnCo<sub>2</sub>O<sub>4</sub>: Charge Separation of the Photo-Generated Electron–Hole Pair. *J. Mater. Sci. Mater. Electron.* **2017**, 28 (1), 289–294.  
<https://doi.org/10.1007/s10854-016-5523-0>.